ability to form pleural effusions in the nude mouse.[21] PC14PE6 and NCI-H441 cell lines were maintained in RPMI 1640 (Gibco, Invitrogen Corporation, Carlsbad, CA, USA) supplemented with 10% FBS (Biosource, USA) supplemented with penicillin (100 U/mL) and streptomycin (100 μg/mL). To create a hypoxic condition of <0.02% of oxygen tension, the cells were treated in an hypoxic chamber, Baclite-1 (Sheldon Manufacturing, Cornelius, OR, USA).

Plasmid constructions. The human HIF-1α was amplified using PCR from HepG2 cDNA. The primer sets used were as follows: forward primer KHIFATG: 5′-AAAAGGTACCATGGAGGGCG-CCGGC-3′, reverse primer HIFTGAN: 5′-CCCGCTAGCTCAGT-TAACTTGATCCAAAGC-3′. PCR products were digested with Kpn I and Nhe I, and subcloned into the Kpn I- and Nhe I-digested pcDNA3.1/v5-His expression plasmid vector (Invitrogen) (designated as pcDNA-HIF-1α). Annealed oligonucleotides for FLAG (5′-CGCCACCATGGACTACAAAGACGATGACGACA-AGGGTAC-3′ and 5′-CCTTGTCGTCATCGTCTTTGTAGTCC-ATGGTGGCGGTAC-3′) were cloned into Kpn I-digested pcDNA-HIF-1α (designated as pcDNA-FLAG-HIF-1α). A construct was confirmed by sequence analyses using T7 and BGH primers with Big Dye Terminators® and ABI Prism 310 Genetic Analyzer® (Applied Biosystems, Foster City, CA, USA).

Gene silencing was performed using the pSuperRetro plasmid purchased from Oligoengine (Seattle, WA, USA). The corresponding sequence of the HIF-1α oligonucleotide 5′-GACA-GTACAGGATGCTTGC-3′[22] was inserted to the plasmid to construct pSR-ND-HIF-1α.

DNA transfection. To establish PC14PE6/EF-Luc and NCI-H441/EF-Luc cell lines, stable DNA transfection was carried out using a calcium phosphate method as described previously.[23] Briefly, PC14PE6 and NCI-H441 cells (10^6/100-mm dish) were transfected with 20 μg pEF/Luc or 5 HRE-hCMVmp/luc plasmid, respectively. The cells were then trypsinized 24 h after transfection and cultured in the selection medium containing 5 μg/mL blasticidin-S or 500 μg/mL G418 (Nacalai Tesque, Kyoto, Japan), respectively, for 10 days. The G418-resistant colonies were isolated and used for *in vitro* cell proliferation assays and mouse xenograft assays.

For transient DNA transfection, cells (1×10^6) were seeded in a 100-mm dish 24 h before transfection. 10 μg of pSR-ND-HIF-1α, pcDNA-FLAG-HIF-1α or an empty vector was cotransfected with 1 μg pFGBH, which encodes EGFP-BSD (blastcidin-S-resistant gene product) fusion protein to check the transfection efficiency, according to the manufacturer's instructions (Biorad, TransFectin™ Lipid Reagent). The medium was replaced with the fresh selection medium containing 500 μg/mL G418 and 5 μg/mL blasticidin-S 6 h after transfection. After incubation for approximately 24 h, the cells were trypsinized and reseeded to several dishes with the selection medium for 2–3 days. They were then examined for luciferase activity, HIF-1α protein expression and sensitivity to PTX. They were incubated for approximately 10–12 h before either hypoxic or normoxic incubation for 24 h. The experiments were done in triplicate and each experiment was repeated at least three times.

Luciferase activity assay. 10^5 cells were seeded onto 24-well plaques in 1 mL 10% FBS RPMI 1640 medium, and cultured overnight, then further cultured under the normoxic or hypoxic condition for 24 h. The cells were then washed with PBS and lyzed with 100 μL passive lysis buffer (Promega, Madison, WI, USA) under normoxic or hypoxic conditions. Luciferase activity was measured using a luminometer (Lumat LB 9507; Berthold, Bad Wildbad, Germany) after the addition of 20 μL of a substrate reagent (luciferin; Promega) to 10 μL of cell lysate.

Western blotting analysis. Cells were harvested and lyzed with 100 μL of western lysis buffer (50 mM Tris [pH 7.5], 1% NP-40, 0.25% SDC, 150 mM NaCl, 1 mM EGTA). The cells cultured under hypoxic conditions were treated in the hypoxic chamber. The cell lysates were sonicated for 5 min and then centrifuged at 10 000*g* for 30 min. The supernatant was assayed to determine protein concentration and 30 μg per lane was applied to SDS-polyacrylamide electrophoresis (10% for HIF-1α and 12.5% for β-tubulin and GAPDH). The protein was then transferred to a nitrocellulose filter (Hybond-ECL; GE Healthcare Biosciences, Piscataway, NJ, USA) and the resultant filter was blocked with 5% non-fat milk in PBS. For detection of HIF-1α and GAPDH, the filters were probed with monoclonal anti-HIF-1α antibody (1:500, BD Bioscience Pharmingen, San Diego, CA, USA), mouse monoclonal anti-β-tubulin antibody (1:1000, Convance, CA, USA) and polyclonal anti-GAPDH antibody (1:1000, Santa Cruz Biotechnology, Santa Cruz, CA, USA), and incubated overnight at 4°C. Then HP-linked secondary antibodies against antimouse and antirabbit IgG (GE Healthcare Biosciences) were incubated for 1 h at room temperature. Detection was carried out with a chemiluminescence-based method using the ECL Plus western blotting detection system (GE Healthcare Biosciences).

FACS analysis of PTX sensitivity. Cells (3×10^5/300 μL) were seeded into 24-well plates. The following day, in case of hypoxic conditions, the cells were preincubated in a hypoxic chamber for 6 h, various concentration of PTX were added to the culture medium and incubated for another 48 h. Then the cells were harvested, gently suspended in PBS and mixed with an equal volume of 2 × hypotonic fluorochrome solution (100 μg/mL propidium iodide in 0.2% sodium citrate–0.2% Triton X-100) immediately before the analysis with flow cytometry using CELLQuest (BD Biosciences, Franklin Lakes, NJ, USA). The population of the cells with degraded smaller genomic DNA (subG1 fraction) was determined using CELLQuest Analysis (Becton Dickinson) and indicated as a percentage of dead cells.

Animals and orthotopic transplantation. Cultured PC14PE6/EF-Luc cells and NCI-H441/EF-Luc cells were harvested by exposure to 0.25% trypsin–0.02% EDTA solution. The cells were washed twice in PBS and resuspended in growth factor-reduced Matrigel (0.5 mg/mL) in PBS. Cell viability was determined using the trypan blue exclusion test and only single-cell suspensions of >90% viability were used for *in vivo* studies. 7–8-week old male athymic nude mice (BALB/c nu/nu; Japan SLC Inc., Hamamatsu, Japan) were anesthetized using sodium pentobarbital (50 mg/kg body weight) and placed into the right lateral decubitus position. The skin over the left chest wall was cut between the 4th and 5th intercostal spaces at the midaxillar line and lung cancer cells (PC14PE6/EF-Luc cell: 1×10^6 in 50 μL; NCI-H441/EF-Luc cell: 5.0×10^4 in 50 μL) were injected into the left lung through the left chest wall using a 30-gauge needle following the method of Onn *et al.*[24] After injection the skin was closed with wound clips.

***In vivo* imaging and PTX treatment.** For the *in vivo* imaging of bioluminescence, the tumor-bearing mice were intraperitoneally injected with 200 μL of D-luciferin solution (10 mg/mL in PBS; Xenogen, Alameda, CA, USA) 20 min before imaging. The animals were then applied to the IVIS™ 200 Imaging System (Xenogen) to monitor the cells in solid tumor. The luciferase activity was calculated as the externally detected photon count, using Living Image Software 2.20 (Xenogen). When tumor formation was confirmed by imaging, the mice were randomized into four groups ($n = 8$) as follows: saline-treated control (PC14PE6 and NCI-H441 xenograft); PTX-alone treatment. PTX (10 mg/kg) was given by intraperitoneal injection every 5 days for 3 or 4 times, beginning after the confirmation of tumor uptake by imaging. Body weights and photon counts were monitored every other day after the initial treatment. The ethical committee of the Kyoto University Institute of Laboratory Animals approved the study.

Immunofluorescence analysis. After transient transfection and culture for 48 h with the selection medium, cells were seeded on Laboratory-Teck chamber slides (Nalge Nunc International, Naperville, IL, USA) and incubated at 37°C with 5% CO_2 overnight.

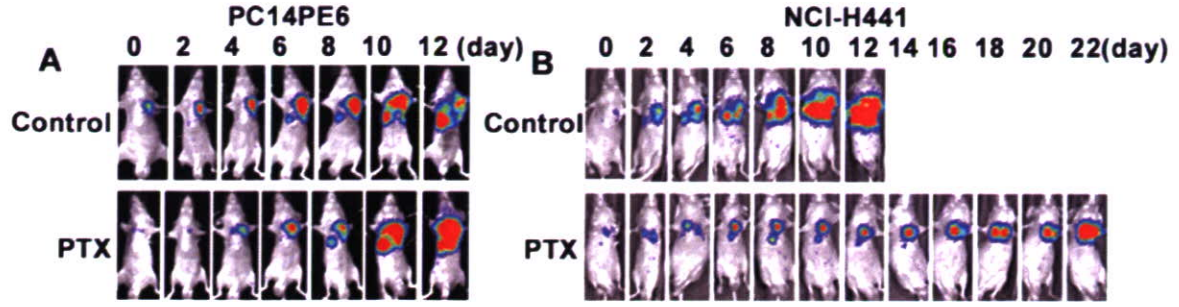

Fig. 1. Optical imaging of PC14PE6 and NCI-H441 cells in orthotopic lung cancer models. (A) PC14PE6/EF-Luc and (B) NCI-H441/pEF-Luc cells were injected into the left lung. When tumor formation was confirmed by bioluminescent images, the mice were randomized into paclitaxel (PTX)-treated (PTX) and untreated (control) groups. The images were taken on the indicated day, in which day 1 is the first treated day. The mice in the figure are representative of each group.

Table 1. Median survival time of PC14PE6/EF-Luc and NCI-H441/EF-Luc orthotopic lung cancer models

Cell type	Treatment group	No. of mice	Median survival time (days ± SD)
PC14PE6/EF-Luc	Control (saline)	9	12 ± 1.49
	Paclitaxel	9	13 ± 1.49
NCI-H441/EF-Luc	Control (saline)	13	12 ± 4.39
	Paclitaxel	11	22 ± 9.34†

†$P < 0.05$ versus control group.

Cells were treated in the annormoxic chamber for 24 h and then they were fixed with 4% paraformaldehyde for 15 min and permeabilized with 0.2% Triton X-100/PBS for 4 min. Immunostaining was performed by incubating the slides with mouse monoclonal antibody polymerized β-tubulin (1:1000; Convance), followed by incubation with Alexa Fluor 488 goat antimouse fluorescent antibody (1:100; Invitrogen) for 1 h at room temperature. As a negative control, slides were incubated with normal goat serum instead of the primary antibodies. Photos were taken under inverted fluorescent microscope (Biozero, Keyence, Japan).

Statistical analysis. Data are expressed as means ± SEM. Statistical significance of differences was determined using a paired two-tailed Student's *t*-test and a log-rank test for the survival curve. Differences were considered statistically significant at $P < 0.05$.

Results

***In vivo* imaging of PTX effects on the PC14PE6 and NCI-H441 orthotopic lung cancer models.** To analyze tumor progression and antitumor effects of PTX in orthotopically transplanted human lung cancer cell lines, PC14PE6 and NCI-H441, it was first established that the transfectants were stably expressing firefly luciferase. This enabled non-invasive monitoring of the orthotopically transplanted xenografts by detecting bioluminescence from the outside with an *in vivo* imaging device. The transfectants grew with a similar speed to their corresponding parental cell lines (data not shown). The cells were injected into the left lung through the left chest wall and bioluminescence externally detected from the xenografts was monitored daily. The typical time course of tumor progression in both NCI-H441 and PC14PE6 lung cancer was the following: the images were detected in the left lung 1 week after transplantation; the image spread to the right lung during the second week; the mice died during the third week (Fig. 1, control groups). When photon counts of tumors were approximately 5×10^4 (6, 7 days after transplantation), the mice were randomized to start the PTX treatment. PTX was intraperitoneally injected every 5 days for 3 or 4 times. Body weights and photon counts of bioluminescence from the tumors were monitored every 2 days after the initial treatment. The image appearance and the photon counts during the experimental period were not significantly different between the untreated and PTX-treated groups in PC14PE6 xenografts (Figs 1,2A). In addition, there was no significant difference in the mean survival time between untreated and PTX-treated groups in PC14PE6 xenografts (Fig. 2C and Table 1). In contrast, the increases in images and photon counts were significantly delayed in the PTX-treated group compared to the untreated group in NCI-H441 xenografts (Figs 1,2B). Furthermore, the mean survival of PTX-treated NCI-H441-tumor bearing mice was prolonged to 22 days compared with 12–13 days in untreated NCI-H441-tumor bearing mice and in both untreated and PTX-treated PC14PE6-tumor bearing mice (Fig. 2C,D and Table 1). There was no significant body-weight loss associated with the treatments (data not shown). These data indicate that NCI-H441 cells are sensitive to PTX *in vivo* but PC14PE6 cells are not.

Effects of PTX on the PC14PE6 and NCI-H441 cells *in vitro*. To investigate the effects of PTX on PC14PE6 and NCI-H441 cells *in vitro*, they were treated with various concentrations of PTX. The effect of PTX on cell death was examined using FACS analysis, in which cells with degraded genome DNA corresponds to the sub-G1 fraction (Fig. 3A). PTX induces polymerization of tubulin and thus blocking of the cell cycle in the M phase,[25] It was found that PTX did not induce cell death to PC14PE6 cells under both hypoxic and normoxic conditions, even at 100-nM PTX concentration (Fig. 3A). At this concentration, PC14PE6 significantly increased G2/M population (Fig. 3C). In contrast to PC14PE6, NCI-H441 cells showed significant sensitivity to PTX under normoxic conditions. Even 0.01 nM PTX induced NCI-H441 to cell death and increased G2/M population under normoxic conditions (Fig. 3B,C). Under hypoxic conditions, however, both PC14PE6 and NCI-H441 cells showed significant resistance to PTX (Fig. 3B,C).

Suppression of HIF-1α expression with siRNA increases the sensitivity to PTX of PC14PE6 cells. Because HIF-1 is the major regulator in

doi: 10.1111/j.1349-7006.2007.00537.x

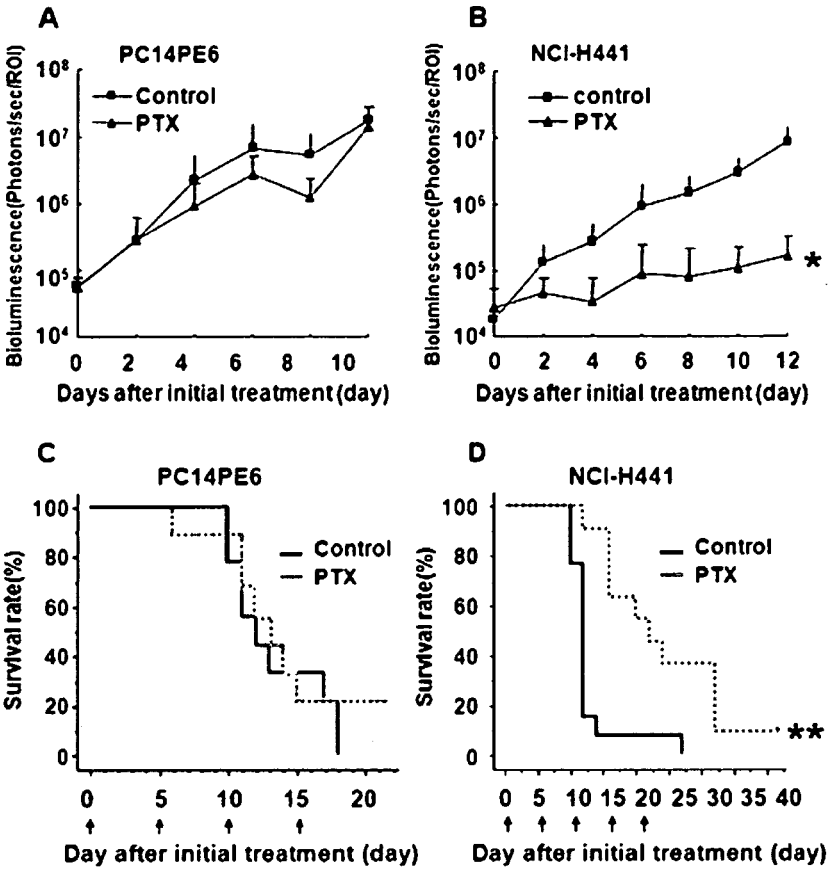

Fig. 2. Effects of paclitaxel (PTX) on PC14PE6 and NCI-H441 tumor xenografts. (A, B) The bioluminescence intensity in (A) PC14PE6/EF-Luc and (B) NCI-H441/EF-Luc xenografts treated with PTX (PTX) and untreated (control) were monitored every other day and quantified as photons/s/ROI. Each group consisted of at least 8 mice and the average photon counts ± SD of each group are shown. $*P < 0.05$ versus control group of NCI-H441 xenografts. (C, D) Survival rate of (C) PC14PE6/EF-Luc and (D) NCI-H441/EF-Luc orthotopic xenografts treated with PTX (PTX) and untreated (control) are shown. $**P < 0.01$ versus control group of NCI-H441 xenografts. The median survival time of each treatment group is shown in Table 1.

hypoxia, the authors investigated whether HIF-1 activity was related to the resistance to PTX. The HIF-1α protein expression level in PC14PE6 and NCI-H441 cells was examined first and it was found that PC14PE6 expressed a significantly higher level of HIF-1α than NCI-H441 cells even under normoxic conditions (Fig. 4).

To further analyze the correlation between HIF-1 and PTX sensitivity in PC14PE6 and NCI-H441 cells, the influence of HIF-1α expression levels on PTX sensitivity of these cells was examined next.

HIF-1α expression in PC14PE6 cells was suppressed with an siRNA specific to HIF-1α. When a plasmid expressing siRNA specific to HIF-1α was transfected to PC14PE6 cells, the HIF-1α protein levels were significantly reduced (Fig. 5A). FACS analysis revealed that PC14PE6 cells with reduced HIF-1α expression significantly increased the sensitivity to PTX compared to the cells transfected with an empty vector (Fig. 5B, $P < 0.05$).

Forced expression of HIF-1α reduced the sensitivity to PTX of NCI-H441 cells. When a plasmid encoding HIF-1α was transfected to NCI-H441 cells, the HIF-1α protein levels were significantly increased (Fig. 6A). The HIF-1α overexpressing NCI-H441 cells were significantly more resistant to PTX than the cells transfected with a control plasmid (Fig. 6A, $P < 0.05$). Together, these results suggest that HIF-1 activity influences the sensitivity to PTX.

HIF-1 influences the conformation of β-tubulin. To investigate the mechanism by which HIF-1 influenced the PTX sensitivity in these cells, their β-tubulin expression was first examined. The β-tubulin protein level was not significantly different between PC14PE6 and NCI-H441 cells under both normoxic and hypoxic conditions (Fig. 7A). Then the β-tubulin distribution in the cells was examined using immunohistochemical analysis (Fig. 7B). In PC14PE6 cells, reduced expression of HIF-1α resulted in flatter morphology and less-assembled β-tubulin under normoxic conditions (Fig. 7, upper left panels). In contrast, forced expression of HIF-1α in NCI-H441 cells resulted in more round morphology and more bundled β-tubulin under normoxic conditions (Fig. 7, upper right panels). All the cells appeared flatter under hypoxic conditions compared to the corresponding cells under normoxic conditions (Fig. 7, lower panels).

Discussion

The authors demonstrate here that the HIF-1α expression level influences the sensitivity of human cancer cell lines, PC14PE6 and NCI-H441, to PTX. The endogenous HIF-1α protein level in PC14PE6 is significantly higher than that of NCI-H441 (Fig. 4), which corresponds to their PTX sensitivity, that is, PC14PE6 is more resistant to PTX than NCI-H441 *in vivo* (Fig. 1) as well as *in vitro* (Fig. 3). Furthermore, when HIF-1α expression was suppressed by siRNA, PC14PE6 increased sensitivity to PTX (Fig. 5), while increased expression of HIF-1α in NCI-H441 resulted in increased resistance to PTX (Fig. 6). The authors have repeatedly observed that the suppression of HIF-1α expression by siRNA slightly decreased the viability of PC14PE6 cells under normoxic conditions (Fig. 6B). In a pancreatic cell line, AsPC-1, the knockdown of HIF-1α also induced minor cell death even under normoxic conditions (M. Inoue *et al.*, unpublished data, 2007).

Although reduced HIF-1α expression by itself influenced the viability of cancer cells, it significantly enhanced the cell death of PTX-treated PC14PE6 cells (Fig. 5B). These results suggest that HIF-1 is one of the factors influencing PTX sensitivity of cancer cells under normoxic conditions. HIF-1α expression

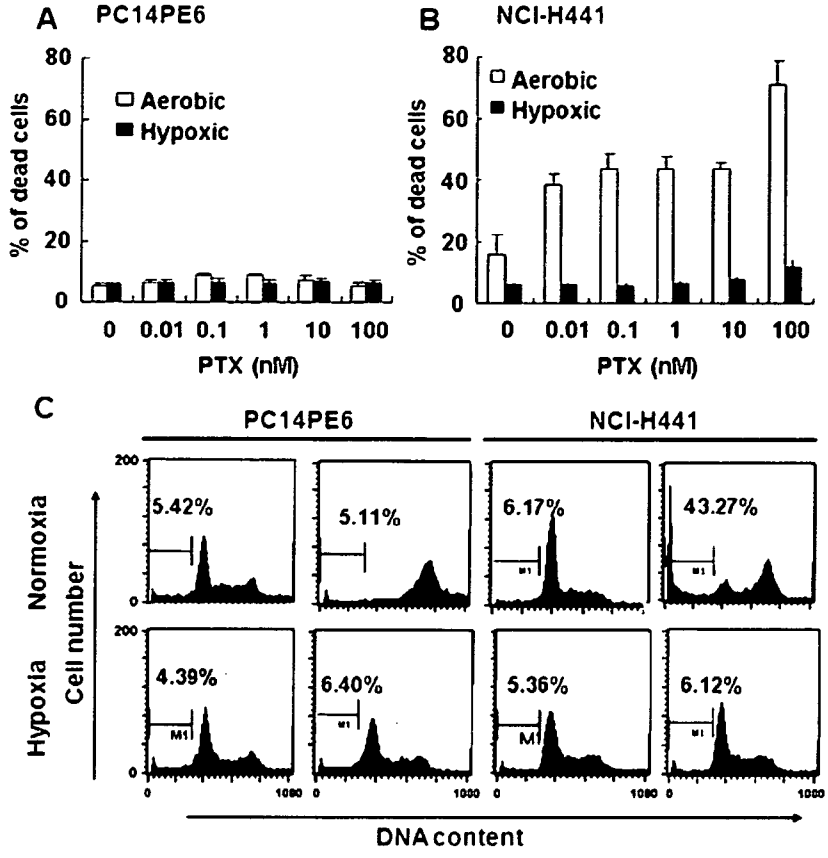

Fig. 3. Effects of paclitaxel (PTX) on PC14PE6 and NCI-H441 cell lines *in vitro*. (A) PC14PE6/EF-Luc and (B) NCI-H441/EF-Luc cells were seeded into 24-well plates and the following day various concentrations of PTX (as indicated) were added to the culture medium and incubated for another 48 h under normoxic or hypoxic conditions. The percentage of dead cells with degraded genomic DNA was analyzed using fluorescence-activated cell sorting (FACS) after staining genomic DNA with propidium iodide. Each experiment was done in triplicate and the average dead cell percentage in each group is shown. Experiments were repeated more than three times and representative data is shown. Error bars indicate SEM. (C) Representative FACS data of each group.

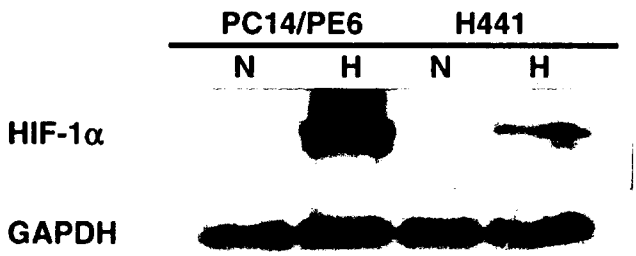

Fig. 4. Western blot analysis of hypoxia inducible factor (HIF)-1α protein expression in the PC14PE6 and NCI-H441 cells. The cells were cultured under normoxic (N) and hypoxic (H) conditions for 24 h and then cells were harvested and lyzed with western lysis buffer under normoxic or hypoxic conditions. The lysates were subjected to an immunoblotting analysis with anti-HIF-1α and anti-glyceraldehyde-3-phosphate dehydrogenase (GAPDH) antibodies as described in Materials and Methods.

levels did not influence the expression level of tubulin protein (Fig. 7A), but did influence the cellular distribution of tubulin and consequently cell morphology (Fig. 7B), suggesting that HIF-1 influenced the conformation of tubulin in these cells. All the cells appeared flatter under hypoxic conditions. These phenomena have been observed not only in cancer cells but also in other types of cells and have been explained by hypoxia-induced alterations in cytoskeletal fiber, actin and tubulin, and extracellular components such as metalloproteinase.[26,27] A recent study strongly supported the role of hypoxia in cytoskeleton changes, as it showed that hypoxia increased tubulin stabilization and changed vesicle trafficking.[27]

Several studies support the notion that the cell cycle plays also a critical role in chemosensitivity for combination chemotherapy. PTX-induced apoptosis can occur either directly after a mitotic arrest[28] or following an aberrant mitotic exit into a G1-like 'multinucleate state.'[25,28,29] Under normoxic conditions, both NCI-H441 and PC14PE6 cells increased G2/M population when treated with PTX (Fig. 3C), while their destinies were different. Under hypoxic conditions, however, they were arrested in neither G1 nor G2/M, suggesting that the effects of PTX under hypoxic conditions might be completely different from those under normoxic conditions. Substantial evidence indicates that the G2/M arrest of the cell cycle is not the only mechanism for PTX-induced apoptosis.[30–33] Additional signal transduction pathways are also involved in inducing apoptosis.[34,35] Further study should be done to clarify the mechanisms resistant to PTX under hypoxic conditions.

Although it is not known how HIF-1 influences the conformation of tubulin, previous reports have suggested some possible mechanisms for the association between HIF-1α and PTX resistance. At present, the best-described mechanism of resistance to tubulin-binding agents is the MDR pump model. In a number of cases,[36–38] development of cell lines resistant to paclitaxel has been shown to be associated with the expression of *MDR1*. But little is known concerning the significance of the MDR phenotype in the emergence of resistant tumors in patients treated with tubulin-binding agents. Clinical trials that have aimed to sensitize MDR-positive tumors to agents such as vinblastine with P-gp modulators have been disappointing.[4]

doi: 10.1111/j.1349-7006.2007.00537.x

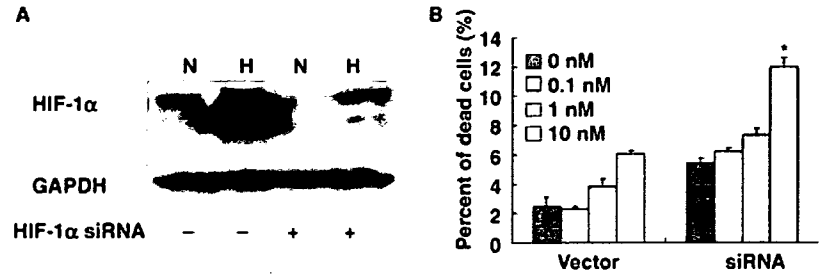

Fig. 5. Suppression of hypoxia inducible factor (HIF)-1α expression with siRNA increases the sensitivity to paclitaxel (PTX) of PC14PE6. (A) The cells were transfected with plasmids encoding enhanced green fluorescent protein (EGFP) and siRNA specific to HIF-1α (+) or empty vector (–) and cultured under normoxic (N) or hypoxic (H) conditions for 48 h with selection medium. The cells were harvested at the end of the culture period and lyzed with western blot buffer under normoxic or hypoxic conditions, respectively. Western blotting was done as described in the legend for Fig. 4. (B) The cells prepared as for (A) were further treated with PTX for 24 h at the indicated concentration. The cells were harvested at the end of the culture period and the DNA contents of EGFP-positive cells were analyzed using fluorescence-activated cell sorting (FACS) as described in the legend for Fig. 3AB. $*P < 0.05$ versus control group. Experiments were repeated in triplicate more than three times and representative data is shown. Error bars indicate SEM.

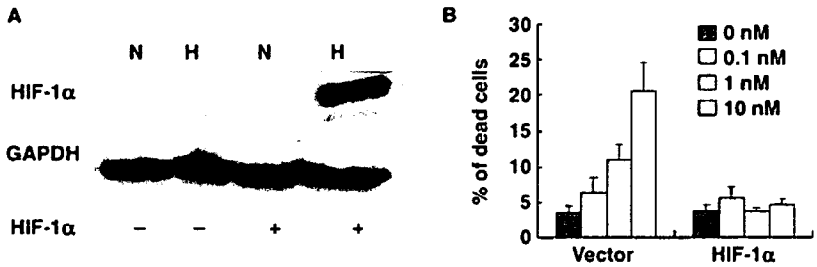

Fig. 6. Forced expression of hypoxia inducible factor (HIF)-1α reduced the sensitivity to paclitaxel (PTX) of NCI-H441 cells. (A) The cells were transfected with plasmids encoding enhanced green fluorescent protein (EGFP) and HIF-1α (+) or empty vector (–) and cultured under normoxic (N) or hypoxic (H) conditions for 48 h with selection medium. The cells were harvested at the end of the culture period and lyzed with western blot buffer under normoxic or hypoxic conditions. Western blotting was done as described in the legend for Fig. 4. (B) The cells prepared as for (A) were further treated with PTX for 24 h at the indicated concentration. The cells were harvested at the end of the culture period and the DNA contents of EGFP-positive cells were analyzed using fluorescence-activated cell sorting (FACS) as described in the legend for Fig. 3AB. Experiments were repeated in triplicate more than three times and representative data is shown. Error bars indicate SEM.

Comerford *et al.* found that HIF-1 induced *MDR1* gene expression and concomitant functional P-gp expression in both transformed epithelia and primary cultured endothelia and suggested that P-gp expression represented a pathway for resistance of some tumors to chemotherapeutics.[9] Therefore, the authors examined P-gp expression in PC14PE6 and NCI-H441 under both normoxic and hypoxic conditions. However, P-gp protein was not detected in either cell lines under both conditions, although other cancer cell lines such as HepG2 expressed a significant amount of P-gp protein under both conditions (data not shown). In these human cancer cell lines, P-gp seems not to contribute to PTX resistance.

Another explanation includes the impacts of HIF-1α-induced downstream genes on the cell cycle and apoptosis-associated pathways. HIF-1α can influence the product of the tumor suppressor gene *p53*,[39,40] which can induce programmed cell death by regulating proteins such as Bax, or cause growth arrest that is mediated by *p21*. It has been shown that HIF-1α directly binds to the *p53* ubiquitin ligase mdm2 both *in vivo* and *in vitro*, thereby stabilizing *p53*.[41] However, there has also been a report that showed direct binding of *p53* to the oxygen-dependent degradation domain of HIF-1α.[42] HIF-1α interacts with wild-type *p53* but not with tumor-derived mutant *p53*.[42] This suggests that the contribution of differing *p53* status of cells might affect their response to stress factors such as PTX treatment for cancer cells. Thus the status of the *p53* gene might play a role in the difference in PTX resistance in PC14PE6 and NCI-H441 because PC14PE6 is wild-type *p53* and NCI-H441 has a mutant-type *p53*.[43] Whether the difference in *p53* status in PC14PE6 and NCI-H441 plays a role or not in the association between PTX and HIF-1α in the present experiments has not been revealed. Further study should be done to clarify this issue.

PTX resistance is also explained based on the dynamics of microtubules.[44] Cabral described a PTX resistance model of 'hypostable' and 'hyperstable' microtubules.[45] Hypostable microtubules tend toward depolymerization spontaneously, and hyperstable microtubules are relatively resistant to depolymerization. Cells with hypostable microtubules are hypersensitive to the depolymerizing agents such as vinca alkaloids while resistant to microtubule stabilizing agents such as PTX. Conversely, cells containing hyperstable microtubules are resistant to the vinca alkaloids but relatively sensitive to PTX. Jordan and Wilson suggested another model.[46] They analyzed the dynamic behavior of individual microtubules and found that PTX at low concentrations reduces microtubule dynamics without significant alteration in microtubule length. According to this explanation, the cells with highly dynamic microtubules are more sensitive to the microtubule-stabilizing agents such as PTX than the cells with less dynamic microtubules.

Although the authors do not know the mechanism by which HIF-1 changes the stability and dynamics of microtubules, it is speculated that unknown factors induced by HIF-1 may influence the conformation and/or dynamics of microtubules. Therefore, it is expected that HIF-1 targeted approaches in combination with PTX may contribute to improve outcome of PTX treatment.

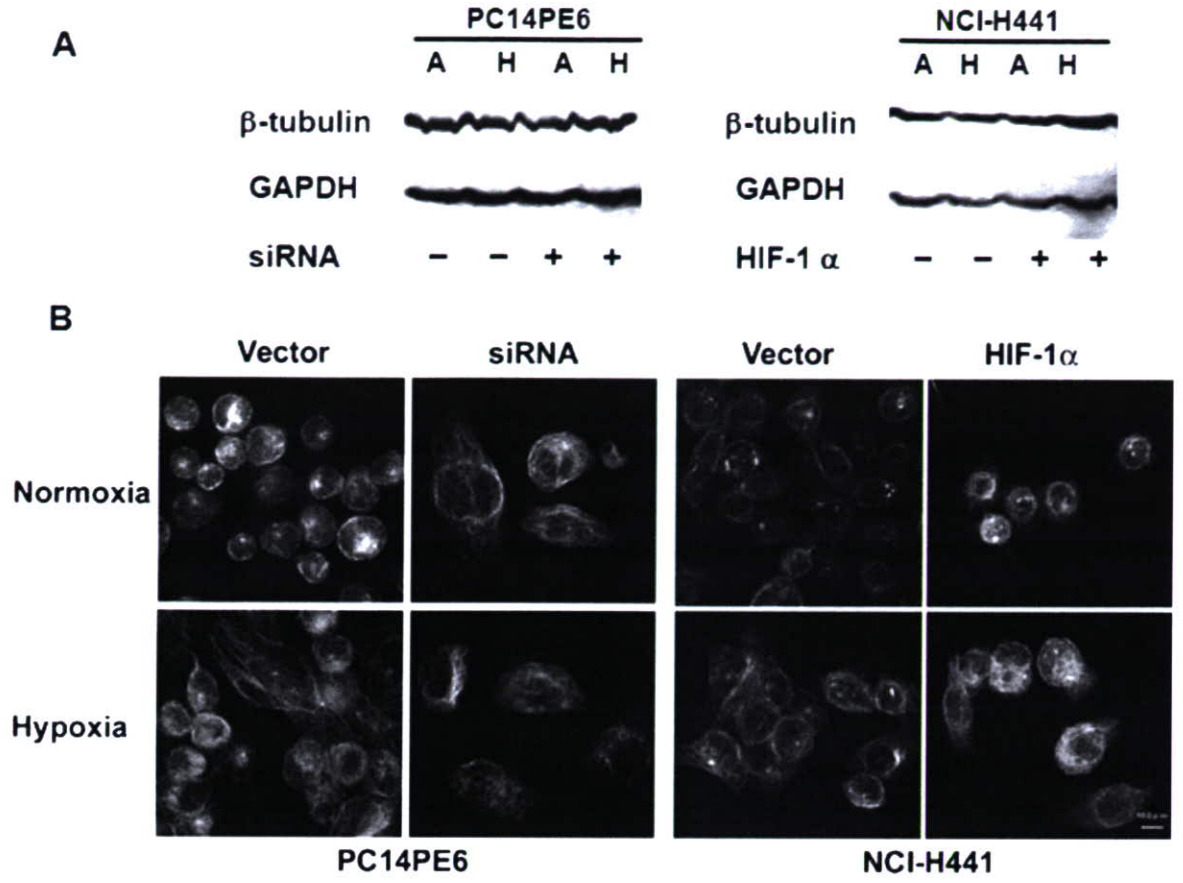

Fig. 7. Influence of hypoxia inducible factor (HIF)-1α expression on β-tubulin conformation. (A) β-tubulin protein expression in the PC14PE6 and NCI-H441 cells. The cells were transfected with plasmids encoding enhanced green fluorescent protein (EGFP) and siRNA specific to HIF-1α (+) or empty vector (–) to PC14PE6 or HIF-1α (+) or empty vector (–) to NCI-H441 and cultured under normoxic (N) or hypoxic (H) conditions for 48 h with selection medium. Cells were harvested and lyzed with western lysis buffer under normoxic or hypoxia conditions, then subjected to immunoblotting with anti-β-tubulin and anti-glyceraldehyde-3-phosphate dehydrogenase (GAPDH) as described in Materials and Methods. (B) Immunofluorescence analysis of polymerized β-tubulin protein expression in PC14PE6 and NCI-H441 cell lines. After transient transfection and culture for 48 h with the selection medium, cells were seeded on chamber slides and incubated overnight. Cells were treated in the annormoxic chamber for 24 h and immunofluorescence analysis was carried out on human lung cancer cell lines, PC14PE6 and NCI-H441, with the combination of polymerized β-tubulin antibody as described in Materials and Methods. Representative results from three independent experiments are shown. Scar bar = 10 μm.

Acknowledgments

This work was supported in part by a Grant-in-Aid for Scientific Research on Priority Areas, Cancer, from the Ministry of Education, Culture, Sports, Science and Technology, and by a Grant-in-Aid for the Third Term Comprehensive 10-Year Strategy for Cancer Control from the Ministry of Health, Labor and Welfare, Japan. This study is a part of joint research which is focusing on the development of the basis of technology for establishing COE for nano-medicine, carried out through Kyoto City Collaboration of Regional Entities for Advancing Technology Excellence (CREATE) assigned by the Japan Science and Technology Agency (JST).

References

1 Miller ML, Ojima I. Chemistry and chemical biology of Taxane anticancer agents. *Chem Record* 2001; **1**: 195–211.
2 Blagosklonny MV, Fojo T. Molecular effects of paclitaxel: myths and reality (a critical review). *Int J Cancer* 1999; **83**: 151–6.
3 Schiff PB, Fant J, Horwitz SB. Promotion of microtubule assembly *in vitro* by Taxol. *Nature* 1979; **277**: 665–7.
4 Dumontet C, Sikic BI. Mechanisms of action of and resistance to antitubulin agents: microtubule dynamics, drug transport, and cell death. *J Clin Oncol* 1999; **17**: 1061–70.
5 Yusuf RZ, Duan Z, Lamendola DE *et al*. Paclitaxel resistance: molecular mechanisms and pharmacologic manipulation. *Curr Cancer Drug Targets* 2003; **3**: 1–19.
6 Sangrajranga S, Fellousb A. Taxol resistance. *Chemotherapy* 2000; **46**: 327–34.
7 Escuin D, Kline ER, Giannakakou P. Both microtubule-stabilizing and microtubule-destabilizing drugs inhibit hypoxia-inducible factor-1alpha accumulation and activity by disrupting microtubule function. *Cancer Res* 2005; **65**: 9021–8.
8 Mabjeesh NJ, Escuin D, LaVallee TM *et al*. 2ME2 inhibits tumor growth and angiogenesis by disrupting microtubules and dysregulating HIF. *Cancer Cell* 2003; **3**: 363–75.
9 Comerford KM, Wallace TJ, Karhausen J, Louis NA, Montalto MC, Colgan S. Hypoxia-inducible factor-1-dependent regulation of the multidrug resistance (MDR1) gene. *Cancer Res* 2002; **62**: 3387–94.
10 Unruh A, Ressel A, Mohamed HG *et al*. The hypoxia-inducible factor-1 is a negative factor for tumor therapy. *Oncogene* 2003; **22**: 3213–20.
11 Erler JT, Cawthorne CJ, Williams KJ *et al*. Hypoxia-mediated down-regulation

doi: 10.1111/j.1349-7006.2007.00537.x

of Bid and Bax in tumors occurs via HIF-1-dependent and -independent mechanisms and contributes to drug resistance. *Mol Cell Biol* 2004; **24**: 2875–89.
12 Semanza GL. Targeting HIF-1 for cancer therapy. *Nat Rev Cancer* 2003; **3**: 721–32.
13 Brown JM, Wilson WR. Exploring tumor hypoxia in cancer treatment. *Nat Rev Cancer* 2004; **4**: 437–47.
14 Kurokawa T, Miyamoto M, Kato K *et al.* Overexpression of hypoxia-inducible-factor 1 alpha (HIF-1alpha) in oesophageal squamous cell carcinoma correlates with lymph node metastasis and pathologic stage. *Br J Cancer* 2003; **89**: 1042–7.
15 Lidgren A, Hedberg Y, Grankvist K, Rasmuson T, Vasko J, Ljungberg B. The expression of hypoxia-inducible factor 1 alpha is a favorable independent prognostic factor in renal cell carcinoma. *Clin Cancer Res* 2005; **11**: 1129–35.
16 Swinson DE, Jones JL, Cox G, Richardson D, Harris AL, O'Byrne KJ. Hypoxia-inducible factor-1 alpha in non small cell lung cancer: relation to growth factor, protease and apoptosis pathway. *Int J Cancer* 2004; **111**: 43–50.
17 Fillies T, Werkmeister R, Van Diest PJ, Brandt B, Joos U, Buerger H. HIF 1-alpha overexpression indicates a good prognosis in early stage squamous cell carcinomas of the oral floor. *BMC Cancer* 2005; **5**: 84–92.
18 Brown LM, Cowen RL, Debray C *et al.* Reversing hypoxic cell chemoresistance in vitro using genetic and small molecule approaches targeting hypoxia inducible factor-1. *Mol Pharmacol* 2006; **69**: 411–18.
19 Unruh A, Ressel A, Mohamed HG *et al.* The hypoxia-inducible factor-1 alpha is a negative factor for tumor therapy. *Oncogene* 2003; **22**: 3213–20.
20 Huang L, Ao QL, Li F, Xing H, Lu YP. Impact of hypoxia on taxol-induced apoptosis in human ovarian cancer cell line A2780 and its mechanism. *Ai Zheng* 2005; **24**: 408–13.
21 Yano S, Herbst RS, Shinohara H *et al.* Treatment for malignant pleural effusion of human lung adenocarcinoma by inhibition of vascular endothelial growth factor receptor tyrosine kinase phosphorylation. *Clin Cancer Res* 2000; **6**: 957–65.
22 Li L-M, Lin X-Y, Staver M *et al.* Evaluating hypoxia-inducible factor-1 as a cancer therapeutic target via inducible RNA interference in vivo. *Cancer Res* 2005; **65**: 7249–58.
23 Harada H, Kizaka-Kondoh S, Hiraoka M. Optical imaging of tumor hypoxia and evaluation of efficacy of a hypoxia-targeting drug in living animals. *Mol Imaging* 2005; **4**: 182–93.
24 Onn A, Isobe T, Itasaka S *et al.* Development of an orthotopic model to study the biology and therapy of primary human lung cancer in nude mice. *Clin Cancer Res* 2003; **9**: 5532–9.
25 Rahat MA, Marom B, Bitterman H, Weiss-Cerem L, Kinarty A, Lahat N. Hypoxia reduces the output of matrix metalloproteinase-9 (MMP-9) in monocytes by inhibiting its secretion and elevating membranal association. *J Leukoc Biol* 2006; **79**: 706–18.
26 Yoon S-O, Shin S, Mercurio AM. Hypoxia stimulates carcinoma invasion by stabilizing microtubules and promoting the Rab11 trafficking of the 6β4 integrin. *Cancer Res* 2005; **65**: 2761–9.
27 Woods CM, Zhu J, McQueney PA, Bollag D, Lazarides E. Taxol-induced mitotic block triggers rapid onset of a p53-independent apoptotic pathway. *Mol Med* 1995; **1**: 506–26.
28 Long BH, Fairchild CR. Paclitaxel inhibits progression of mitotic cells to G1 phase by interference with spindle formation without affecting other microtubule functions during anaphase and telophase. *Cancer Res* 1994; **54**: 4355–61.
29 Lin HL, Chang YF, Liu TY, Wu CW, Chi CW. Submicromolar paclitaxel induces apoptosis in human gastric cancer cells at early G1 phase. *Anticancer Res* 1998; **18**: 3443–9.
30 Milross CG, Mason KA, Hunter NR, Chung WK, Peters LJ, Milas L. Relationship of mitotic arrest and apoptosis to antitumor effect of paclitaxel. *J Natl Cancer Inst* 1996; **88**: 1308–14.
31 Milas L, Hunter NR, Kurdoglu B *et al.* Kinetics of mitotic arrest and apoptosis in murine mammary and ovarian tumors treated with Taxol. *Cancer Chemother Pharmacol* 1995; **35**: 297–303.
32 Lanni JS, Lowe SW, Licitra EJ, Liu JO, Jacks T. p53-independent apoptosis induced by paclitaxel through an indirect mechanism. *Proc Natl Acad Sci USA* 1997; **94**: 9679–83.
33 Moos PJ, Fitzpatrick FA. Taxane-mediated gene induction is independent of microtubule stabilization: induction of transcription regulators and enzymes that modulate inflammation and apoptosis. *Proc Natl Acad Sci USA* 1998; **95**: 3896–901.
34 Blagosklonny MV, Giannakakou P, el-Deiry WS *et al.* Raf-1/bcl-2 phosphorylation: a step from microtubule damage to cell death. *Cancer Res* 1997; **57**: 130–5.
35 Haldar S, Jena N, Croce CM. Inactivation of Bcl-2 by phosphorylation. *Proc Natl Acad Sci USA* 1995; **92**: 4507–11.
36 Horwitz SB, Liao LL, Greenberger L *et al.* Mode of action of Taxol and characterization of multidrug-resistant cell line resistant to Taxol. In: Kessel D, ed. *Resistance to Antineoplastic Drugs*. Boca Raton, FL: CRC Press, 1989; 109–26.
37 Breier A, Barancik M, Sulova Z, Uhrik B. P-glycoprotein-implications of metabolism of neoplastic cells and cancer therapy. *Curr Cancer Drug Targets* 2005; **5**: 457–68.
38 Lorico A, Rappa G, Flavell RA *et al.* Double knockout of the MRP gene leads to increased drug sensitivity in vitro. *Cancer Res* 1996; **56**: 5351–5.
39 Ravi R, Mookerjee B, Bhujwalla ZM *et al.* Regulation of tumor angiogenesis by p53-induced degradation of hypoxia-inducible factor 1a. *Gene Dev* 2000; **14**: 34–44.
40 Hansson LO, Friedler A, Freund S *et al.* Two sequence motifs from HIF-1 alpha bind to the DNA-binding site of p53. *Proc Natl Acad Sci USA* 2002; **99**: 10 305–9.
41 Chen D, Li M, Luo J *et al.* Direct interactions between HIF-1 alpha and Mdm2 modulate p53 function. *J Biol Chem* 2003; **278**: 13 595–8.
42 An WG, Kanekal M, Simon MC *et al.* Stabilization of wild-type p53 by hypoxia-inducible factor 1 alpha. *Nature* 1998; **392**: 405–8.
43 Lai S-L, Perng R-P, Hwang J. p53 Gene status modulates the chemosensitivity of non-small cell lung cancer cells. *J Biomed Sci* 2000; **7**: 64–70.
44 Verdier-Pinard P, Wang F, Martello L, Burd B, Orr GA, Horwitz SB. Analysis of tubulin isotypes and mutations from taxol-resistant cells by combined isoelectrofocusing and mass spectrometry. *Biochemistry* 2003; **42**: 5349–57.
45 Cabral F. Factors determining cellular mechanisms of resistance to antimitotic drugs. *Drug Resist Updat* 2001; **4**: 3–8.
46 Jordan MA, Wilson L. Microtubules and actin filaments: dynamic targets for cancer chemotherapy. *Curr Opin Cell Biol* 1998; **10**: 123–30.

Hypoxia and Hypoxia-Inducible Factor-1 Expression Enhance Osteolytic Bone Metastases of Breast Cancer

Toru Hiraga,[1,2] Shinae Kizaka-Kondoh,[3] Kiichi Hirota,[4] Masahiro Hiraoka,[3] and Toshiyuki Yoneda[1]

[1]Department of Biochemistry, Graduate School of Dentistry, Osaka University, Suita, Osaka, Japan; [2]Department of Histology and Cell Biology, Matsumoto Dental University, Shiojiri, Nagano, Japan; [3]Department of Therapeutic Radiation Oncology, Kyoto University Graduate School of Medicine; and [4]Department of Anesthesia, Kyoto University Hospital, Kyoto, Japan

Abstract

Hypoxia is a common feature of solid tumors and is associated with their malignant phenotype. The transcription factor hypoxia-inducible factor-1 (HIF-1) is a major regulator of adaptation to hypoxia and is implicated in the malignant progression of cancers. Here, we studied whether hypoxia and HIF-1 expression contribute to the development of bone metastases using a well-characterized animal model of bone metastasis in MDA-MB-231 human breast cancer cells. To study the role of hypoxia in bone metastases, we tested the effects of the fusion protein (TOP3), the oxygen-dependent degradation domain of HIF-1α fused with HIV-TAT, and procaspase-3. TOP3 selectively induced apoptosis in hypoxic tumor cells *in vitro* and significantly reduced bone metastases *in vivo*. We next examined the role of HIF-1 in bone metastases by establishing MDA-MB-231 cells overexpressing constitutively active or dominant-negative HIF-1α (MDA/CA-HIF or MDA/DN-HIF, respectively). Bone metastases of MDA/CA-HIF were significantly increased with elevated number of CD31-positive blood vessels. In contrast, bone metastases were significantly reduced in MDA/DN-HIF. Because the progression of osteolytic bone metastases is due in part to the imbalance between bone formation and bone resorption, we examined the effects of hypoxia and HIF-1 on the differentiation of osteoblasts and osteoclasts. Hypoxia and CA-HIF overexpression markedly inhibited osteoblastic differentiation, whereas hypoxia increased osteoclast-like cell formation. In conclusion, these results suggest that tumor-associated hypoxia and HIF-1 expression promote the progression of bone metastases in breast cancer. Our results also suggest that hypoxia and HIF-1 lead to the development of osteolytic bone metastases by suppressing osteoblast differentiation and promoting osteoclastogenesis. [Cancer Res 2007;67(9):4157–63]

Introduction

Hypoxia is a common feature of solid tumors, which is caused by reduced or inadequate oxygen supply (1–3). According to Vaupel et al. (4), median tumor oxygen concentration in breast cancer is ~1.3%, which is much lower than the surrounding normal tissue. Tumor hypoxia has been considered to be a potential therapeutic problem because hypoxic tumor cells are resistant to radiotherapy and chemotherapy (1–3). Furthermore, recent studies suggest that tumor hypoxia is associated with malignant biological phenotype, including enhanced invasiveness, angiogenesis, and distant metastasis (1–3).

The transcription factor hypoxia-inducible factor-1 (HIF-1), which consists of a heterodimer of HIF-1α and HIF-1β, is a major regulator for cancer cells to adapt hypoxia (2, 5). More than 60 putative direct HIF-1 target genes, including glycolytic enzymes, glucose transporter, angiogenic factors, growth factors, enzymes, and proteins involved in tumor invasiveness and metastasis, and apoptosis resistance–related proteins, have been identified (2, 5). HIF-1α possesses a unique oxygen-dependent degradation domain (ODD) that controls protein stability (2, 5, 6). Under normoxia, HIF-1α is continuously degraded by ubiquitin-proteasome pathway, which specifically targets the ODD. On the other hand, under hypoxia, HIF-1α is stabilized, dimerizes with HIF-1β, and initiates gene transcription. Clinicopathologic studies have shown that the expression level of HIF-1α in breast cancer increases as the pathologic stage elevates (7). Furthermore, increased levels of HIF-1α are associated with increased proliferation, metastasis, and poor prognosis in breast cancer patients (8–10).

Bone is one of the most common sites of metastases in breast cancer (11). Bone metastases are usually associated with devastating complications, including severe bone pain, pathologic bone fracture, hypercalcemia, and nerve compression syndromes, and causes increased morbidity and eventual mortality in breast cancer patients (11). In the present study, we studied whether hypoxia and HIF-1 contribute to the development of bone metastases using an animal model of human breast cancer. To examine the role of hypoxia in bone metastases, we used a fusion protein, which comprised of the protein transduction domain (PTD) embedded in the HIV-TAT protein, ODD, and procaspase-3 [*T*AT-PTD-*O*DD-*P*rocaspase-*3* (TOP3); refs. 2, 12]. It has been shown that HIV-TAT fusion protein can be delivered to all tissues, including brain, and used to deliver functional biomolecules *in vivo* (13). Of note, because this fusion protein contains ODD, it is degraded under the normoxic condition; however, under the hypoxic condition, the protein is stabilized and causes caspase-3–induced cell death. We previously showed that the TAT-ODD fusion protein was accumulated specifically in the hypoxic regions in tumors (12). Furthermore, TOP3 selectively killed the hypoxic cells and suppressed the tumor growth in mice (12). To examine the role of HIF-1 in bone metastases, we established MDA-MB-231 human breast cancer cells stably transfected with constitutively active or dominant-negative HIF-1α cDNA (MDA/CA-HIF or MDA/DN-HIF, respectively; refs. 14, 15). The effects of YC-1, an inhibitor of HIF-1 (16), on bone metastases of MDA-MB-231 were also studied. It is well known that the bone metastases of breast cancer are predominantly osteolytic (11); however, the mechanisms are not fully understood. To approach this, we studied the effects of hypoxia and HIF-1 on bone cells, osteoblasts, and osteoclasts, *in vitro*.

Note: Supplementary data for this article are available at Cancer Research Online (http://cancerres.aacrjournals.org/).

Requests for reprints: Toshiyuki Yoneda, Department of Biochemistry, Graduate School of Dentistry, Osaka University, 1-8 Yamadaoka, Suita, Osaka 565-0871, Japan. Phone: 81-6-6879-2887; Fax: 81-6-6879-2890; E-mail: tyoneda@dent.osaka-u.ac.jp.

doi:10.1158/0008-5472.CAN-06-2355

Materials and Methods

Reagents

Mouse monoclonal anti–HIF-1α antibody and rat monoclonal anti-CD31 antibody were purchased from BD Biosciences. Rabbit polyclonal anti-poly(ADP-ribose) polymerase (PARP) antibody and mouse monoclonal anti-FLAG antibody were from Stressgen Bioreagents Corp. and Sigma, respectively. YC-1 [3-(5′-hydroxymethyl-2′-furyl)1-benzylindazole; ref. 16] was from Alexis Corp. Recombinant human bone morphogenetic protein 2 (BMP2) was obtained as described previously (17). All other chemicals used in this study were purchased from Sigma or Wako Pure Chemical Industries, Ltd., unless otherwise described.

Cell Culture

The human breast cancer cell line MDA-MB-231 (American Type Culture Collection) was cultured in DMEM (Sigma) supplemented with 10% FCS (Asahi Glass Techno Corp.) and 100 μg/mL kanamycin sulfate (Meiji Seika Kaisha, Ltd.). C3H10T1/2 cells were purchased from RIKEN BioResource Center and cultured in α-MEM (Sigma) supplemented with 10% FCS and 100 μg/mL kanamycin sulfate. Mouse primary osteoblasts were isolated as described previously (17). All cells were maintained in a humidified atmosphere of 5% CO_2 in air. Hypoxia was achieved by incubating cells in a humidified environment at 37°C in a CO_2 incubator (ASTEC Co., Ltd.) maintained at 94% N_2, 5% CO_2, and 1% O_2.

TAT Fusion Protein

TOP3 and TAT-PTD-ODD fused to β-galactosidase (TAT-PTD-ODD-β-Gal) were prepared as previously described (12). For X-gal staining, TAT-ODD-β-Gal (1 unit of β-Gal activity/mL) was added to subconfluent MDA-MB-231 cells in 24-well plates and the cells were cultured for 24 h. X-gal staining was done as described previously (12).

Western Blot

Whole-cell lysates and nuclear extracts were prepared as described previously (17, 18). Equivalent amounts were loaded for SDS-PAGE, and immunoblotting was done (17, 18). We confirmed that equal amounts of proteins were loaded by staining the transferred membranes with Ponceau S.

Apoptosis

Subconfluent MDA-MB-231 cells in six-well plates were treated with TOP3 (15 μg/mL) for 36 h. Apoptosis in MDA-MB-231 cells were determined using a fluorescence-activated cell sorting (FACS) technique as previously described (18). The percentages of sub-G_1 nuclei in the population were determined as percentage apoptosis.

Transfection

The cDNAs encoding constitutively active (14) and dominant-negative (15) forms of HIF-1α ligated into pcDNA3 (Invitrogen) and p3XFLAG-CMV10 vector (Sigma) were transfected into MDA-MB-231 cells using FuGENE 6 Transfection Reagent (Roche Diagnostics Co.) according to the manufacturer's protocol (MDA/CA-HIF and MDA/DN-HIF). As a control, empty pcDNA3 vector was similarly transfected into MDA-MB-231 cells (MDA/EV). Colonies resistant to 1 mg/mL G418 (Sigma) were isolated and cloned.

ELISA

MDA-MB-231 cells (1×10^4) were plated in 48-well plates. When near confluence, the cells were rinsed with PBS and 250 μL of serum-free DMEM was added to each well. The conditioned medium was collected after 48 h. Concentrations of vascular endothelial growth factor (VEGF) in the conditioned medium were determined by ELISA (R&D Systems, Inc.) according to the manufacturer's instruction. Data are expressed as amount of VEGF produced (pmol/L/mL) per 10^5 cells.

Animal Experiments

Under the anesthesia with pentobarbital (0.05 mg/g body weight; Dainippon Pharmaceutical Co., Ltd.), parental MDA-MB-231, MDA/EV, MDA/CA-HIF, or MDA/DN-HIF cells (1×10^5/0.1 mL PBS) were injected into the left cardiac ventricle of nude mice (female, 4-week-old, SLC Japan Co., Ltd.) as previously described (18). TOP3 (2 or 20 mg/kg) was i.p. injected on days 14, 18, 22, and 26. YC-1 (30 mg/kg) was i.p. injected daily for 2 weeks from day 14 (16). In all experiments, mice were sacrificed at day 28. The number of mice used in each experiment was described in each figure. All animal experiments were reviewed by the Institutional Review Board of Animal Experiments in Osaka University Graduate School of Dentistry.

X-ray Analysis of Osteolytic Lesion Area

Areas of osteolytic lesions were determined on radiographs as described previously (18). Radiographs were analyzed carefully by two different individuals who had no prior knowledge of the experimental protocol. Data are shown as osteolytic lesion area (mm^2)/mouse.

Histologic and Immunohistochemical Analysis

Paraffin sections of the femora and tibiae were made as previously described (18).

Detection of hypoxia. The hypoxic regions in the bone metastases were detected using Hypoxyprobe-1 kit (Chemicon International, Inc.) according to the manufacturer's protocol. Briefly, the tumor-bearing mice were i.p. injected with pimonidazole hydrochloride (60 mg/kg) and were sacrificed 2 h later. The accumulation of pimonidazole was visualized by the immunohistochemical technique.

Immunohistochemistry. Immunohistochemical staining of HIF-1α and CD31 was done using VECTASTAIN Elite ABC kit (Vector Laboratories, Inc.) according to the manufacturer's protocol. Chromogen was developed using 3,3′-diaminobenzidine substrate kit (Vector Laboratories). The slides were counterstained with hematoxylin.

Enzyme histochemistry. Tartrate-resistant acid phosphatase (TRAP) and alkaline phosphatase activities were detected by histochemical staining technique as described previously (18, 19).

Histomorphometric Analysis

Tumor burden. Histomorphometric analysis of tumor burden in bone was done as described previously (18). Data are shown as tumor area (mm^2) / animal.

Microvessel density. CD31-positive microvessels were counted in five random fields at ×200 magnification. Data are shown as the number of CD31-positive microvessels/mm^2 tumor area.

All of the histomorphometric analyses were done extensively and carefully by two different individuals, all of whom were without knowledge of the experimental protocol.

Adenovirus

The recombinant adenovirus carrying CA-HIF-1α was constructed using Adenovirus Expression Vector Kit (TAKARA Bio, Inc.) according to the manufacturer's protocol. As a control, the adenovirus carrying enhanced green fluorescent protein (EGFP) was used. The viruses showed no proliferative activity due to a lack of E1A-E1B (20). Titers of the viruses were determined by a modified point assay (20).

Alkaline Phosphatase Staining

C3H10T1/2 cells (1×10^4 per well/48-well plate) were cultured in the presence of 100 ng/mL BMP2 for 7 days under 20% or 1% O_2. The cells were stained with a mixture of 330 μg/mL nitroblue tetrazolium, 165 μg/mL bromochoroindoylphosphate, 100 mmol/L NaCl, 5 mmol/L $MgCl_2$, and 100 mmol/L Tris (pH 9.5).

Alizarin Red Staining

Mouse primary osteoblasts (1×10^4 per well/48-well plate) were cultured in the presence of 100 ng/mL BMP2, 5 mmol/L β-glycerophosphate, and 100 μg/mL ascorbic acid for 14 days under 20% or 1% O_2. The cells were rinsed twice with PBS, fixed in 10% buffered formalin, and stained with 1% alizarin red solution for 5 min.

Reverse Transcription PCR

Total RNA was isolated using TRI Reagent (Sigma) and single-strand cDNA was synthesized using BD PowerScript Reverse Transcriptase (BD Biosciences). The primer sets used for PCR were as follows: mouse Runx2,

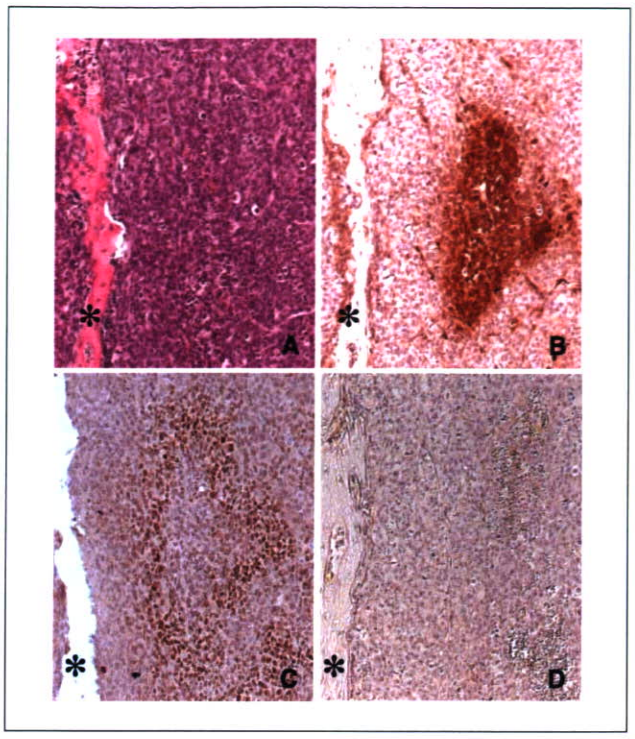

Figure 1. Hypoxia and HIF-1α expression in bone metastases of MDA-MB-231 human breast cancer cells in nude mice. Hypoxia (*B*) was determined by the accumulation of pimonidazole as described in Materials and Methods. HIF-1α expression (*C*) was determined by immunohistochemistry. (*A*, H&E staining; *D*, negative control of HIF-1α immunohistochemistry; *, bone; original magnification, ×200).

GCCGGGAATGATGAGAACTA/GGACCGTCCACTGTCACTTT; mouse osteocalcin, AAGCAGGAGGGCAATAAGGT/ACTTGCAGGGCAGAGAGAGA; mouse glyceraldehyde-3-phosphate dehydrogenase (GAPDH), TTGAAGGGTGGAGCCAAACG/ACACATTGGGGGTAGGAACACG. PCR products were separated on 2% agarose gels containing ethidium bromide and visualized under UV light. The size of the fragments was confirmed by reference to 100-bp DNA ladder. Quantification of amplified mRNA was done by densitometry assisted by the image analysis software Scion Image (Scion Corporation).

Osteoclast Differentiation *In vitro*

Spleen cells were isolated from ddY mice (male, 4-week-old, SLC Japan) and cultured in αMEM supplemented with 10% FCS, 30 ng/mL recombinant human macrophage colony-stimulating factor (M-CSF; Peprotech EC, Ltd.), and 50 ng/mL recombinant human soluble receptor activator of nuclear factor-κB ligand (sRANKL; Peprotech EC) for 6 days under normoxia or hypoxia. At the end of the culture, the cells were stained with TRAP, a marker enzyme of osteoclasts using a commercially available kit (Sigma). TRAP-positive multinucleated (three or more nuclei) cells in each well were counted under light microscope. Data are shown as number of TRAP-positive multinucleated cells per well.

Statistical Analysis

Data are expressed as the mean ± SE and were analyzed by one-way ANOVA followed by Fisher's protected least-significant differences post hoc test (StatView; SAS Institute, Inc.) for determination of differences between groups. Student's *t* test or Welch's *t* test was conducted when two groups were compared. *P* values of <0.05 were considered significant.

Results

Hypoxia in bone metastases of MDA-MB-231 human breast cancer cells. To rationalize the use of the animal model of MDA-MB-231 human breast cancer cells in this study, we first determined the presence of hypoxic regions in the bone metastases using a hypoxic marker pimonidazole. Immunohistochemical study showed the accumulation of pimonidazole in MDA-MB-231 cells colonized in bone (Fig. 1). Because pimonidazole accumulates in the cells that have oxygen concentration <10 mmHg pO_2, which corresponds to ~1.3% O_2 in the gas phase (2), the result suggests that the bone metastases in this animal model include equivalent levels of hypoxic regions to human breast cancers (4).

Effects of TOP3 on bone metastases of MDA-MB-231 cells. To study the role of hypoxia in bone metastases, we examined effects of TOP3 (12). Consistent with the previous report (12), our *in vitro* study using TAT-PTD-ODD-β-Gal showed that β-Gal activity was markedly increased in MDA-MB-231 cells cultured under the hypoxic condition compared with the cells cultured under normoxia, verifying the

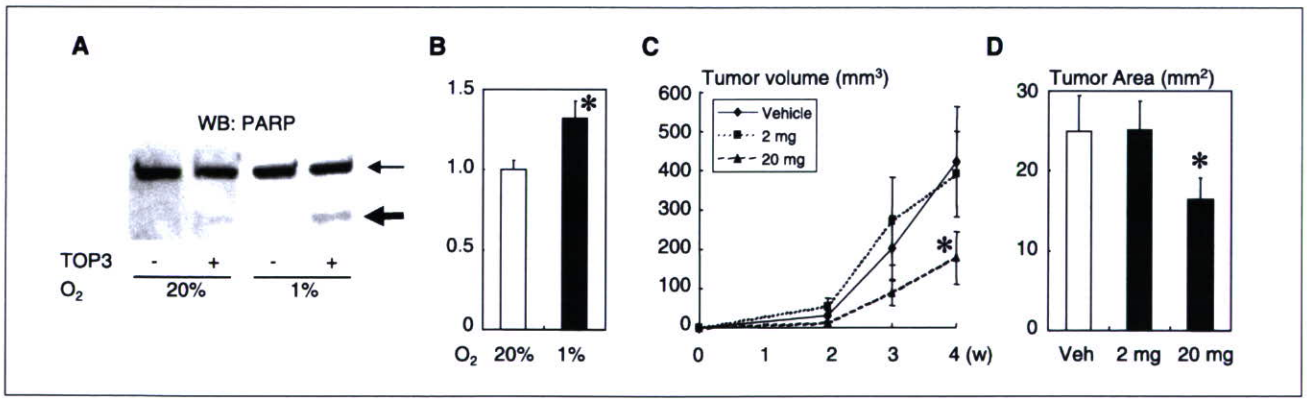

Figure 2. Effects of TOP3 on bone metastases of MDA-MB-231 cells. *A*, effect of TOP3 on the cleavage of PARP in MDA-MB-231 cells determined by Western blot (*WB*). The cells were cultured with TOP3 (15 μg/mL) for 36 h under 20% or 1% O_2 (*thin arrow*, intact PARP; *thick arrow*, cleaved PARP). *B*, effects of TOP3 on apoptosis in MDA-MB-231 cells. The cells were cultured with TOP3 (15 μg/mL) for 36 h under 20% or 1% O_2. Apoptosis was evaluated using FACS as described in Materials and Methods. Data are shown as apoptosis relative to 20% O_2. *C*, effects of TOP3 on the growth of MDA-MB-231 tumors in the orthotopic mammary fat pad. Data are shown as tumor volume (mm^3; n = 9/group). *, $P < 0.05$, significantly different from vehicle. *D*, effects of TOP3 on bone metastases of MDA-MB-231 cells. The metastatic tumor burden in bone was assessed by histomorphometry as described in Materials and Methods. Data are shown as tumor area (mm^2) / mouse (n = 9/group). *, $P < 0.05$, significantly different from vehicle.

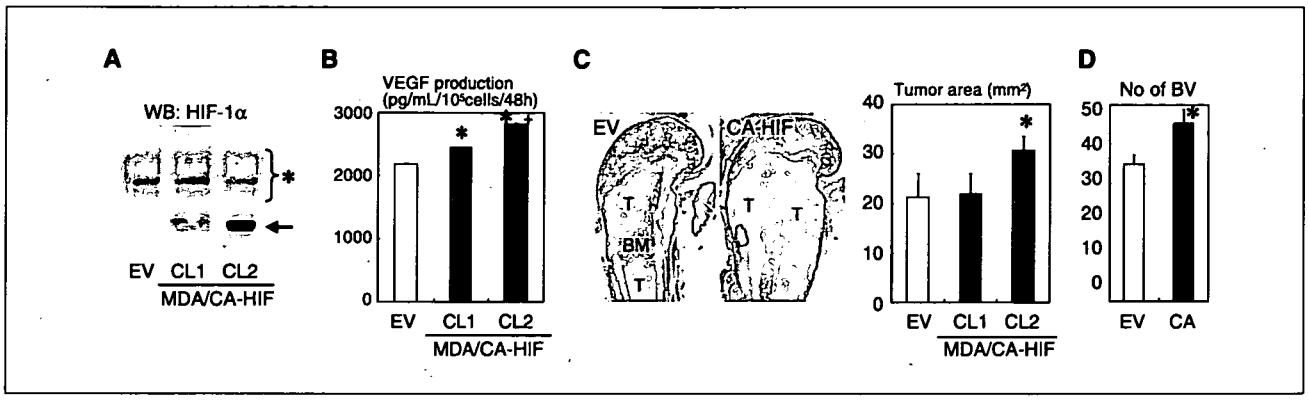

Figure 3. Effects of CA-HIF-1α on bone metastases of MDA-MB-231 cells. *A*, establishment of MDA-MB-231 cells overexpressing CA-HIF-1α (*MDA/CA-HIF*). Expression of CA-HIF-1α was determined by Western blot [*EV*, empty vector-transfected clone; clone 1 (*CL1*); low expression clone; clone 2 (*CL2*), high expression clone; *, endogenous wild-type HIF-1α; *arrow*, CA-HIF-1α]. *B*, VEGF production by MDA/CA-HIF. The cells were cultured with serum-free medium for 48 h under normoxia. The conditioned medium was collected and VEGF concentration was measured by ELISA. *Columns*, amount of VEGF produced (pg/mL/10^5 cells/48 h; n = 3/group). *, $P < 0.01$, significantly different from MDA/EV; +, $P < 0.01$, significantly different from MDA/CA-HIF clone 1. *C*, histomorphometric analysis of tumor burden of MDA/CA-HIF in the hind limbs in nude mice. *Left*, representative histologic view of bone metastases of MDA/EV (*EV*) and MDA/CA-HIF (clone 2; *CA-HIF*). H&E staining: *T*: tumor; *BM*: bone marrow, original magnification, ×25. Tumor burden was determined as described in Materials and Methods. Quantitative data are shown as tumor area (mm^2) / mouse (n = 9/group). *, $P < 0.05$, significantly different from MDA/EV. *D*, histomorphometric analysis of blood vessel density in bone metastases of MDA/CA-HIF (clone 2). Blood vessel density was determined as described in Materials and Methods. Data are shown as number of blood vessels (*BV*) / mm^2 tumor area (n = 9/group). *, $P < 0.05$, significantly different from MDA/EV.

oxygen-dependent stability of TAT-PTD-ODD fusion proteins in MDA-MB-231 cells (Supplementary Fig. S1). We then examined effects of TOP3 on MDA-MB-231 cells *in vitro*. Western blot analysis showed that TOP3 increased the cleavage of a caspase-3 substrate protein PARP in the hypoxic cultures (Fig. 2*A*). Furthermore, apoptosis in MDA-MB-231 cells was significantly increased by the TOP3 treatment under hypoxia (Fig. 2*B*). We further examined the effects of TOP3 on MDA-MB-231 tumors *in vivo*. I.p. administrations of TOP3 inhibited the orthotopic tumor formation and the development of bone metastases in a dose-dependent manner (Fig. 2*C* and *D*).

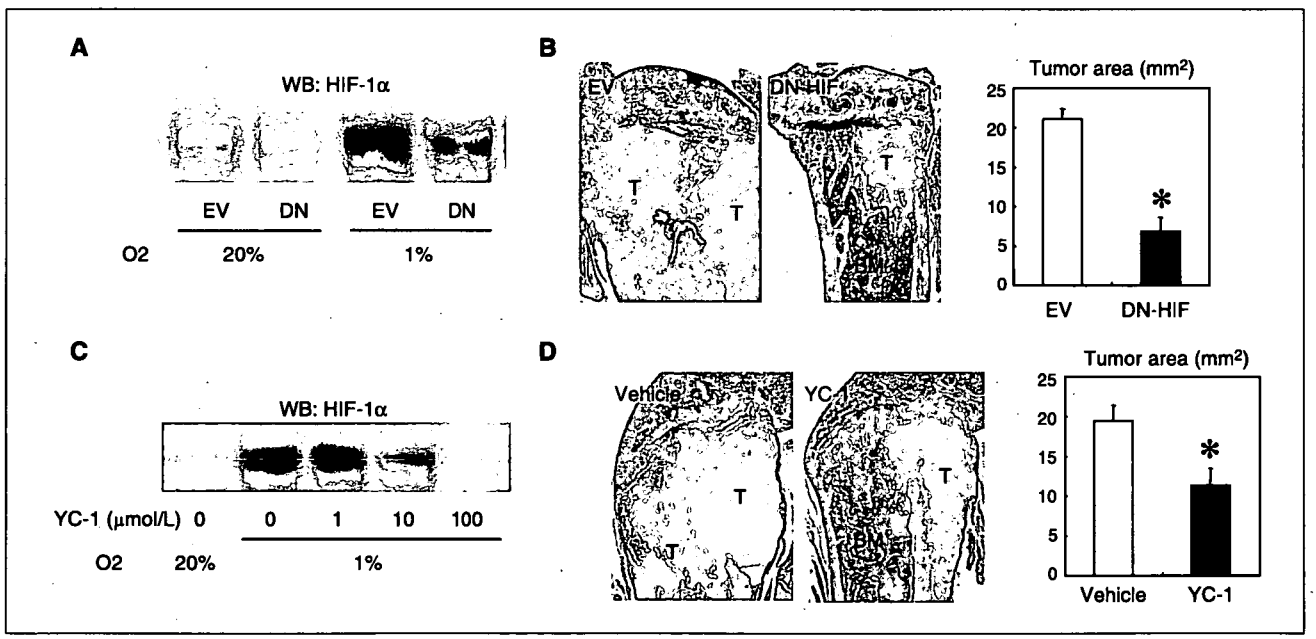

Figure 4. Effects of DN-HIF-1α and YC-1 on bone metastases of MDA-MB-231 cells. *A*, expression of endogenous wild-type HIF-1α in MDA/EV and MDA/DN-HIF (*DN*) under normoxia and hypoxia. *B*, histomorphometric analysis of tumor burden of MDA/DN-HIF in the hind limbs in nude mice. *Left*, representative histologic view of bone metastases of MDA/EV and MDA/DN-HIF (*DN-HIF*). H&E staining: *T*: tumor; *BM*: bone marrow, original magnification, ×25. Tumor burden was determined as described in Materials and Methods. Quantitative data are shown as tumor area (mm^2) / mouse (n = 9/group). *, $P < 0.05$, significantly different from MDA/EV. *C*, effects of YC-1 on nuclear HIF-1α expression in parental MDA-MB-231 cells. The cells were treated with YC-1 (1, 10, or 100 μmol/L) 5 min before being cultured under hypoxic conditions for 4 h. *D*, histomorphometric analysis of tumor burden of parental MDA-MB-231 cells in the hind limbs in nude mice treated without or with YC-1. *Left*, representative histologic view of bone metastases of parental MDA-MB-231 cells treated with vehicle or YC-1. H&E staining: original magnification, ×25. Tumor burden was determined as described in Materials and Methods. Quantitative data are shown as tumor area (mm^2) / mouse (n = 5/group). *, $P < 0.05$, significantly different from vehicle.

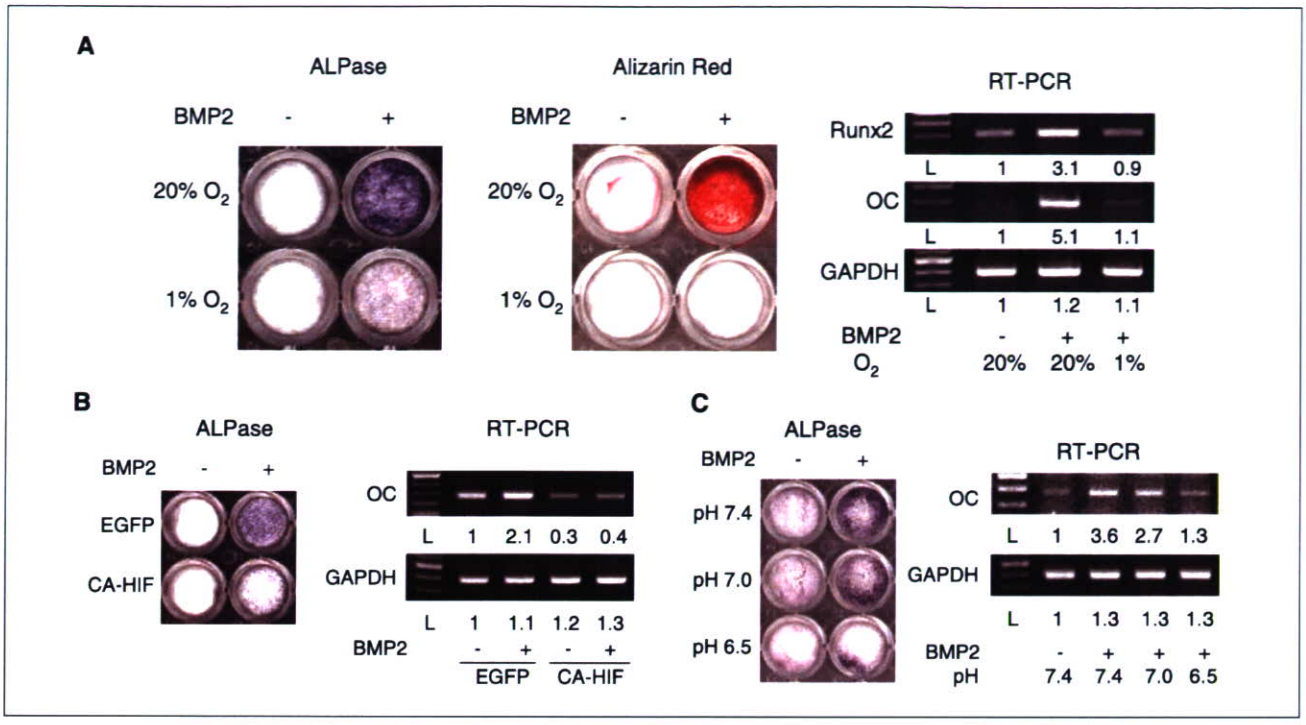

Figure 5. Effects of hypoxia, HIF-1 expression, and acidosis on osteoblast differentiation. *A*, effects of hypoxia on osteoblast differentiation determined by alkaline phosphatase (*ALPase*) activity in C3H10T1/2 cells, alizarin red staining of mouse primary calvarial osteoblasts, and semiquantitative RT-PCR analysis of *Runx2* and *osteocalcin* (*OC*) mRNA expression in C3H10T1/2 cells cultured with or without BMP2 (100 ng/mL) under normoxia or hypoxia. *B*, effects of HIF-1 expression on osteoblast differentiation determined by ALPase activity and *osteocalcin* mRNA expression in C3H10T1/2 cells infected with EGFP or CA-HIF-1α (*CA-HIF*) adenovirus. The cells were cultured with or without BMP2 (100 ng/mL) under normoxia. *C*, effects of acidosis on osteoblast differentiation determined by ALPase activity and *osteocalcin* mRNA expression in C3H10T1/2 cells cultured with the acidic medium in the presence or absence of BMP2 (100 ng/mL) under normoxia. Quantification of amplified mRNA was done as described in Materials and Methods and indicated as fold induction (*L*, 100 bp DNA ladder).

Effects of CA-HIF, DN-HIF, and YC-1 on bone metastases of MDA-MB-231. We then studied the role of HIF-1 in bone metastases. Western blot analysis showed that hypoxia induced HIF-1α accumulation in MDA-MB-231 cells *in vitro* (data not shown). Immunohistochemical study showed that the tumor cells with nuclear HIF-1α expression colocalized or surrounded the pimonidazole-positive cells in the bone metastases of MDA-MB-231 cells in nude mice (Fig. 1*C*). To examine the role of HIF-1 in bone metastases *in vivo*, we established MDA-MB-231 cells stably transfected with CA-HIF-1α cDNA (MDA/CA-HIF). Because CA-HIF-1α lacks the ODD domain (14), it is not degraded even under normoxic condition. Two clones of MDA/CA-HIF with low and high expression levels of CA-HIF-1α were used in the following experiments (Fig. 3*A*). ELISA showed that VEGF production was significantly increased in MDA/CA-HIF cells in a CA-HIF-1α expression–dependent manner (Fig. 3*B*). Radiological and histomorphometric analyses showed that osteolytic lesion area and tumor burden in bone were significantly increased in the high expression clone of MDA/CA-HIF (clone 2) compared with MDA/EV, whereas they were not changed in the low expression clone (clone 1; Fig. 3*C* and Supplementary Fig. S2). Blood vessel density determined by CD31 immunohistochemistry was significantly increased in the bone metastases of the MDA/CA-HIF (Fig. 3*D*).

To further determine the role of HIF-1 in bone metastases, we examined the capacity of MDA-MB-231 cells overexpressing DN-HIF-1α (MDA/DN-HIF; Supplementary Fig. S3) to develop bone metastases in nude mice. Western blot showed that nuclear HIF-1α accumulation was reduced in MDA/DN-HIF under both normoxic and hypoxic conditions (Fig. 4*A*). Histomorphometric examination showed that bone metastases were significantly reduced in MDA/DN-HIF (Fig. 4*B*). We also studied the effects of YC-1, which was shown to have inhibitory effects on the expression of HIF-1α and the induction of HIF-1 target genes, including *VEGF* (16), on bone metastases of MDA-MB-231 cells. YC-1 reduced nuclear HIF-1α expression also in MDA-MB-231 cells in a dose-dependent manner (Fig. 4*C*). Furthermore, YC-1 significantly decreased metastatic tumor burden of MDA-MB-231 cells in bone (Fig. 4*D*).

Effects of hypoxia and HIF-1 on bone cells. In bone metastases, bone cells, including osteoblasts, osteoclasts, and their precursor cells, share the common microenvironment with tumor cells colonized in bone. As shown in Supplementary Fig. S4, alkaline phosphatase–positive spindle-shaped osteoblast precursor cells and TRAP-positive mononuclear osteoclast precursor cells were adjacent to pimonidazole-positive hypoxic MDA-MB-231 cells, suggesting that hypoxia and HIF-1 activation may affect bone metabolism by influencing the differentiation of bone cells. Thus, we finally examined whether hypoxia and HIF-1 contribute to the induction of osteolysis frequently seen in bone metastases of breast cancer by studying their effects on osteoblasts and osteoclasts *in vitro*. The pluripotent mesenchymal cells C3H10T1/2 was shown to differentiate to alkaline phosphatase–positive osteoblast-like cells in the presence of BMP2 (17). Hypoxia markedly inhibited BMP2-induced alkaline phosphatase activity in C3H10T1/2 cells (Fig. 5*A*). BMP2-induced calcification in mouse primary osteoblasts determined by Alizarin red staining was also suppressed by hypoxia (Fig. 5*A*). Semiquantitative reverse transcription-PCR (RT-PCR)

analysis showed that hypoxia reduced BMP2-induced mRNA expression of the osteoblast differentiation markers, *Runx2* and *osteocalcin*, in C3H10T1/2 cells (Fig. 5*A*). Consistent with these results, the introduction of CA-HIF-1α by adenovirus inhibited BMP2-induced osteoblast differentiation and *osteocalcin* mRNA expression in C3H10T1/2 cells (Fig. 5*B*). In contrast, hypoxia increased TRAP-positive osteoclast-like cell formation in spleen cell cultures in the presence of sRANKL and M-CSF (Fig. 6*A*).

Hypoxia is frequently associated with low extracellular pH due to increased production of lactic acid through enhanced glycolysis (3). To approach the mechanisms of the suppressed differentiation of osteoblasts and the enhanced differentiation of osteoclasts under hypoxia, we examined the effects of acidosis on the differentiation of osteoblasts and osteoclasts. BMP2-induced alkaline phosphatase activity in C3H10T1/2 cells was reduced as the extracellular pH decreased (Fig. 5*C*). Acidic pH also suppressed BMP2-induced *osteocalcin* mRNA expression in C3H10T1/2 cells (Fig. 5*C*). In contrast, sRANKL and M-CSF–induced osteoclast differentiation in the spleen cell cultures was significantly increased in the low pH culture conditions (Fig. 6*B*).

Discussion

In solid tumors, oxygen delivery to tumor cells is frequently reduced by deteriorating diffusion geometry, severe structural abnormalities of microvessels, and disturbed microcirculation, leading to induce hypoxia. Previous reports using clinical samples showed that median tumor oxygen concentrations are generally lower than the surrounding normal tissues (1). Although the oxygen concentrations in bone metastases in cancer patients have not been explored yet, our immunohistochemical study using the hypoxic marker pimonidazole showed the presence of hypoxic regions in the bone metastases of MDA-MB-231 human breast cancer cells in nude mice. Because tissue oxygenation is associated with tumor size (2), our data that even relatively small size tumors in mouse bones include substantial hypoxic regions suggest that larger tumor mass in human bones likely have increased volume of hypoxic tumor cells. These results suggest that hypoxia may affect the pathophysiology of bone metastases of breast cancer.

To study the role of hypoxia in bone metastases, we tested the effects of TOP3 in our animal model. When used *in vivo*, the HIV-TAT fusion protein has been shown to be delivered to the entire body, including brain (13). The fusion protein is able to freely diffuse through cell membranes, and therefore through layers of tumor cells. Thus, HIV-TAT fusion proteins can be delivered to tissues where blood vessels are shut down, such as in ischemic brain (21). Consistent with the previous reports (12), our results showed that TOP3 was stabilized and caused caspase-3–induced apoptosis selectively in hypoxic MDA-MB-231 cells. Furthermore, animal experiments showed that the i.p. administration of TOP3 reduced the bone metastases as well as the orthotopic tumors of MDA-MB-231 cells. These results support the notion that hypoxia makes a substantial contribution to the development of bone metastases of breast cancer.

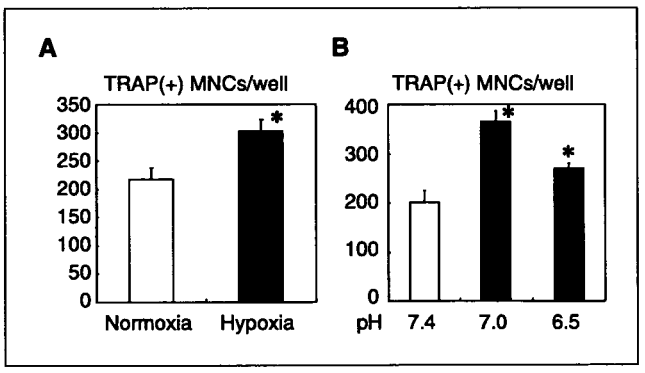

Figure 6. Effects of hypoxia and acidosis on osteoclast differentiation. Osteoclast-like cell formation was determined in spleen cell cultures in the presence of M-CSF (30 ng/mL) and sRANKL (50 ng/mL) under hypoxia (*A*) or acidic pH (*B*). Data are expressed as number of TRAP-positive multinucleated cells (*MNC*) per well per 48-well plate (n = 4/group). *, $P < 0.05$, significantly different from normoxia or pH 7.4.

Hypoxia causes a variety of biological responses in tumor cells. The transcription factor HIF-1 is a master mediator of the hypoxic response of tumor cells and controls the up-regulation of a number of factors vital for tumor expansion, including angiogenic factors such as VEGF. Western blot analysis showed that hypoxia induced HIF-1α accumulation in MDA-MB-231 cells and immunohistochemical study revealed the hypoxia-associated nuclear HIF-1α expression in MDA-MB-231 cells colonized in bone. The localization of the HIF-1α–positive cells and the pimonidazole-incorporated cells was not identical (Fig. 1). However, according to the recent report by Sobhanifer et al. (22), HIF-1α expression is decreased in perinecrotic regions of solid tumors. In addition, pimonidazole accumulates in the cells only below 1.3% O_2. These may account for the discrepancy.

The overexpression of CA-HIF-1α in MDA-MB-231 cells increased the production of one of the HIF-1 target gene product VEGF. Furthermore, CA-HIF-1α enhanced the progression of bone metastases of MDA-MB-231 cells accompanied with the increased number of CD31-positive microvessels. It is well known that angiogenesis is critical to tumor growth, survival, and metastasis (23). The previous reports showed that the inhibitors of angiogenesis reduced bone metastases in animal models (24, 25). These results collectively suggest that the promoted angiogenesis by the elevated VEGF production might play a causative role in the increased tumor burden in MDA/CA-HIF.

Breast cancer frequently causes osteolysis in bone metastases (11). Osteolysis in bone metastasis is thought to be due to the uncoupling between osteoclastic bone resorption and osteoblastic bone formation. It is widely recognized that osteolysis is caused by the production of osteoclast-activating factors such as parathyroid hormone-related protein (11). In addition, recent studies showed that the Wnt signal inhibitors, dickkopf-1 and secreted Frizzled-related protein-2, also play roles in the development of osteolytic lesions in multiple myeloma by inhibiting bone formation (26, 27). Consistent with the previous reports (28, 29), our results showed that hypoxia inhibited osteoblast differentiation of the multipotent mesenchymal cells C3H10T1/2 and mouse primary calvarial osteoblasts *in vitro*. In addition, we showed that the introduction of CA-HIF-1α inhibited osteoblast differentiation of C3H10T1/2 cells, suggesting that hypoxia-induced inhibition of osteoblast differentiation is, at least in part, dependent on HIF-1. We also found that acidosis, which is frequently caused by hypoxia, has a negative effect on osteoblast differentiation as well as osteoblast function (30, 31). The result suggests that hypoxia-induced acidic microenvironment contributes to the inhibition of osteoblast differentiation. In contrast to the effects on osteoblast differentiation, hypoxia stimulated osteoclast-like cell formation in mouse spleen cell culture. Arnett et al. (32) and Fukuoka et al. (33) showed

similar results. Furthermore, acidosis also enhanced osteoclast differentiation in a pH-dependent manner. As the molecular mechanisms of the acidosis-increased osteoclast formation, Frick et al. (34) reported that metabolic acidosis stimulates mRNA expression of *RANKL* in bone cells. Komarova et al. (35) showed that acidosis directly acts on osteoclasts to activate nuclear factor of activated T cells c1, the critical transcription factor to osteoclast differentiation (36). These results collectively suggest that hypoxia and HIF-1 are involved in the formation of osteolytic bone metastases by suppressing osteoblast differentiation and stimulating osteoclast differentiation.

Bone metastasis is often classified as either osteolytic or osteoblastic. Osteoblastic metastases are frequently seen in prostate cancer patients. However, oxygen levels in prostate cancer are comparable or even lower than that in breast cancer (37, 38). Osteoblastic metastasis is believed to be caused by the cancer cell production of factors that stimulate osteoblast proliferation, differentiation, and bone formation. Several lines of experimental evidence have shown that prostate cancer cells promote osteoblastic activity by secreting osteoblast-stimulating factors, including BMPs (39, 40). These results suggest that, in the bone metastases of prostate cancer, these osteoblastic factors may play a dominant role in the formation of osteoblastic metastases even in the hypoxic condition.

In conclusion, the results suggest that tumor-associated hypoxia and HIF-1 expression promote the progression of bone metastases in breast cancer. Our results also suggest that hypoxia and HIF-1 also play a role in the induction of osteolytic change in bone metastases through causing an uncoupling between bone resorption and formation. Hypoxia and HIF-1 may be potential therapeutic targets for bone metastases in breast cancer.

Acknowledgments

Received 6/28/2006; revised 1/11/2007; accepted 2/12/2007.

Grant support: Grants in aid 14771020, 16791123, 18592031 (T. Hiraga), 17014058 and 21st century Center of Excellence program (T. Yoneda) from the Ministry of Education, Culture, Sports, Science and Technology, Japan; Senri Life Science Foundation Research Grant (T. Hiraga); Osaka Cancer Society Research Grant (T. Hiraga); and Research Grant from Sagawa Foundation for Promotion of Cancer Research (T. Hiraga).

The costs of publication of this article were defrayed in part by the payment of page charges. This article must therefore be hereby marked *advertisement* in accordance with 18 U.S.C. Section 1734 solely to indicate this fact.

References

1. Brown JM, Wilson WR. Exploiting tumor hypoxia in cancer treatment. Nat Rev Cancer 2004;4:437–47.
2. Kizaka-Kondoh S, Inoue M, Harada H, Hiraoka M. Tumor hypoxia: a target for selective cancer therapy. Cancer Sci 2003;94:1021–8.
3. Harris AL. Hypoxia—a key regulatory factor in tumor growth. Nat Rev Cancer 2002;2:38–47.
4. Vaupel S, Briest S, Hockel M. Hypoxia in breast cancer: pathogenesis, characterization and biological/therapeutic implications. Wien Med Wochenschr 2002;152:334–42.
5. Semenza GL. Targeting HIF-1 for cancer therapy. Nat Rev Cancer 2003;3:721–32.
6. Huang LE, Bunn HF. Hypoxia-inducible factor and its biomedical relevance. J Biol Chem 2003;278:19575–8.
7. Bos R, Zhong H, Hanrahan CF, et al. Levels of hypoxia-inducible factor-1α during breast carcinogenesis. J Natl Cancer Inst 2001;93:309–14.
8. Zhong H, De Marzo AM, Laughner E, et al. Overexpression of hypoxia-inducible factor 1α in common human cancers and their metastases. Cancer Res 1999;59:5830–5.
9. Gruber G, Greiner RH, Hlushchuk R, et al. Hypoxia-inducible factor 1α in high-risk breast cancer: an independent prognostic parameter? Breast Cancer Res 2004;6:R191–8.
10. Schindl M, Schoppmann SF, Samonigg H, et al. Overexpression of hypoxia-inducible factor 1α is associated with and unfavorable prognosis in lymph node-positive breast cancer. Clin Cancer Res 2002;8:1831–7.
11. Mundy GR. Metastasis to bone: causes, consequences and therapeutic opportunities. Nat Rev Cancer 2002;2:584–93.
12. Harada H, Hiraoka M, Kizaka-Kondoh S. Antitumor effect of TAT-oxygen-dependent degradation-caspase-3 fusion protein specifically stabilized and activated in hypoxic tumor cells. Cancer Res 2002;62:2013–8.
13. Schwarze SR, Ho A, Vocero-Akbani A, Dowdy SF. *In vivo* protein transduction: delivery of a biologically active protein into the mouse. Science 1999;285:1569–72.
14. Kelly BD, Hackett SF, Hirota K, et al. Cell type-specific regulation of angiogenic growth factor gene expression and induction of angiogenesis in nonischemic tissue by a constitutively active form of hypoxia-inducible factor 1. Circ Res 2003;93:1074–81.
15. Kasuno K, Takabuchi S, Fukuda K, et al. Nitric oxide induces hypoxia-inducible factor 1 activation that is dependent on MAPK and phosphatidylinositol 3-kinase signaling. J Biol Chem 2004;279:2550–8.
16. Yeo E-J, Chun Y-S, Cho Y-S, et al. YC-1: a potential anticancer drug targeting hypoxia-inducible factor 1. J Natl Cancer Inst 2003;95:516–25.
17. Ichida F, Nishimura R, Hata K, et al. Reciprocal roles of Msx2 in regulation of osteoblast and adipocyte differentiation. J Biol Chem 2004;279:34015–22.
18. Hiraga T, Myoui A, Choi ME, Yoshikawa H, Yoneda T. Stimulation of cyclooxygenase-2 expression by bone-derived transforming growth factor β enhances bone metastases in breast cancer. Cancer Res 2006;66:2067–73.
19. Ito M, Amizuka N, Tanaka S, et al. Ultrastructural and cytobiological studies on possible interactions between PTHrP-secreting tumor cells, stromal cells, and bone cells. J Bone Miner Metab 2003;21:353–62.
20. Miyake S, Makimura M, Kanegae Y, et al. Efficient generation of recombinant adenoviruses using adenovirus DNA-terminal protein complex and a cosmid bearing the full-length virus genome. Proc Natl Acad Sci U S A 1996;93:1320–4.
21. Asoh S, Ohsawa I, Mori T, et al. Protection against ischemic brain injury by protein therapeutics. Proc Natl Acad Sci U S A 2002;99:17107–12.
22. Sobhanifar S, Aquino-Parsons C, Stanbridge EJ, Olive P. Reduced expression of hypoxia-inducible factor-1a in perinecrotic regions of solid tumors. Cancer Res 2005;65:7259–66.
23. Ferrara N, Kerbel RS. Angiogenesis as a therapeutic target. Nature 2005;438:967–74.
24. Sasaki A, Alcalde RE, Nishiyama A, et al. Angiogenesis inhibitor TNP-470 inhibits human breast cancer osteolytic bone metastasis in nude mice through the reduction of bone resorption. Cancer Res 1998;58:462–7.
25. Weber MH, Lee J, Orr FW. The effects of Neovastat (AE-941) on an experimental metastatic bone tumor model. Int J Oncol 2002;20:299–303.
26. Tian E, Zhan F, Walker R, et al. The role of the Wnt-signaling antagonist DKK1 in the development of osteolytic lesions in multiple myeloma. N Engl J Med 2003;349:2483–94.
27. Oshima T, Abe M, Asano J, et al. Myeloma cells suppress bone formation by secreting a soluble Wnt inhibitor, sFRP-2. Blood 2005;106:3160–5.
28. Park JH, Park BH, Kim HK, Park TS, Baek HS. Hypoxia decreases Runx2/Cbfa1 expression in human osteoblast-like cells. Mol Cell Endocrinol 2002;192:197–203.
29. Salim A, Nacamuli RP, Morgan EF, Giaccia AJ, Longaker MT. Transient changes in oxygen tension inhibit osteogenic differentiation and Runx2 expression in osteoblasts. J Biol Chem 2004;279:40007–16.
30. Tuncay OC, Ho D, Barker MK. Oxygen tension regulates osteoblast function. Am J Orthod Dentofacial Orthop 1994;105:457–63.
31. Warren SM, Steinbrech DS, Mehrara BJ, et al. Hypoxia regulates osteoblast gene expression. J Surg Res 2001;99:147–55.
32. Arnett TR, Gibbons DC, Utting JC, et al. Hypoxia is a major stimulator of osteoclast formation and bone resorption. J Cell Physiol 2003;196:2–8.
33. Fukuoka H, Aoyama M, Miyazawa K, Asai K, Goto S. Hypoxic stress enhances osteoclast differentiation via increasing IGF2 production by non-osteoclastic cells. Biochem Biophys Res Commun 2005;328:885–94.
34. Frick KK, Bushinsky DA. Metabolic acidosis stimulates RANKL RNA expression in bone through a cyclo-oxygenase-dependent mechanism. J Bone Miner Res 2003;18:1317–25.
35. Komarova SV, Pereverzev A, Shum JW, Sims SM, Dixon SJ. Convergent signaling by acidosis and receptor activator of NF-κB ligand (RANKL) on the calcium/calcineurin/NFAT pathway in osteoclasts. Proc Natl Acad Sci U S A 2005;102:2643–8.
36. Takayanagi H, Kim S, Koga T, et al. Induction and activation of the transcription factor NFATc1 (NFAT2) integrate RANKL signaling in terminal differentiation of osteoclasts. Dev Cell 2002;3:889–901.
37. Movsas B, Chapman JD, Greenberg RE, et al. Increasing levels of hypoxia in prostate carcinoma correlate significantly with increasing clinical stage and patient age: an Eppendorf pO_2 study. Cancer 2000;89:2018–24.
38. Movsas B, Chapman JD, Hanlon AL, et al. Hypoxia in human prostate carcinoma: an Eppendorf pO_2 study. Am J Clin Oncol 2001;24:458–61.
39. Dai J, Keller J, Zhang J, Lu Y, Yao Z, Keller ET. Bone morphogenetic protein-6 promotes osteoblastic prostate cancer bone metastases through a dual mechanism. Cancer Res 2005;65:8274–85.
40. Masuda H, Fukabori Y, Nakano K, Takezawa Y, Suzuki T, Yamanaka H. Increased expression of bone morphogenetic protein-7 in bone metastatic prostate cancer. Prostate 2003;54:268–74.

J Neurooncol (2007) 85:95–103
DOI 10.1007/s11060-007-9396-1

CLINICAL–PATIENT STUDY

The lack of expression of the peripheral benzodiazepine receptor characterises microglial response in anaplastic astrocytomas

Shigetoshi Takaya · Kazuo Hashikawa · Federico E. Turkheimer · Nicholas Mottram · Manuel Deprez · Koichi Ishizu · Hidekazu Kawashima · Haruhiko Akiyama · Hidenao Fukuyama · Richard B. Banati · Federico Roncaroli

Received: 26 January 2007 / Accepted: 23 April 2007 / Published online: 23 May 2007

Abstract The peripheral benzodiazepine receptor (PBR) is a 18 kDa molecule mainly involved in cholesterol transport through the mitochondrial membrane. In microglia, PBR is expressed from the earliest stages of activation and appears to exert a pro-inflammatory function. This molecule is commonly up-regulated in inflammatory, degenerative, infective and ischaemic lesions of the central nervous system but it has never been reported in glioma-infiltrating microglia. We examined two anaplastic astrocytomas showing minimal contrast-enhancement and therefore little damage of the blood brain barrier to minimise the presence of blood borne macrophages within tumour tissue. The two lesions were studied in vivo using positron emission tomography (PET) with the specific PBR ligand [^{11}C](R)-PK11195 and the corresponding tumour tissue was investigated with an anti-PBR antibody. Glioma-infiltrating microglia were characterised for molecules involved in antigen presentation and cytotoxic activity. As comparison, PBR was investigated in three brains with multiple sclerosis (MS) and three with Parkinson's disease (PD). The expression profile of four anaplastic astrocytomas was also exploited and results were compared to the profile of eleven samples of normal temporal lobe and nine cases of PD. PET studies showed that [^{11}C](R)-PK11195 binding was markedly lower in tumours than in the contralateral grey matter. Pathological investigation revealed that glioma-infiltrating microglia failed to express PBR and cytotoxic molecules although some cells still expressed antigen presenting molecules. PBR and cytotoxic molecules were highly represented in MS and PD. Evaluation of microarray datasets confirmed these differences. Our results demonstrated PBR suppression in glioma-infiltrating microglia and suggested that PBR may have a relevant role in modulating the anti-tumour inflammatory response in astrocytic tumours.

Keywords Astrocytoma · Microglia · Peripheral benzodiazepine receptor · PK11195 · Positron emission tomography

S. Takaya
Radioisotope Research Centre, Kyoto University, Kyoto, Japan

S. Takaya · K. Hashikawa · H. Fukuyama
Human Brain Research Centre, Kyoto University Graduate School of Medicine, Kyoto, Japan

F. E. Turkheimer
Department of Clinical Neuroscience, Division of Neuroscience, Imperial College London, London, UK

N. Mottram · F. Roncaroli (✉)
University Department of Neuropathology, Division of Neuroscience and Mental Health, Imperial College London, Charing Cross Campus, St Dunstans Road, London W6 8RP, UK
e-mail: f.roncaroli@imperial.ac.uk

M. Deprez
Department of Neuropathology, University of Liege, Liege, Belgium

K. Ishizu · H. Kawashima
Department of Nuclear Medicine and Diagnostic Imaging, Kyoto University Graduate School of Medicine, Kyoto, Japan

H. Akiyama
Tokyo Institute of Psychiatry, Tokyo, Japan

R. B. Banati
School of Medical Radiation Science, Ramaciotti Centre for Brain Imaging at the Brain Mind Research Institute [BMRI], University of Sydney, Sydney, NSW, Australia

Introduction

Microglia are the resident immune cells of the central nervous system (CNS) [1]. They are ubiquitously distributed across brain regions in a "resting" state and constitute a network of surveillance and defence cells, with their cytoplasmic processes continuously scanning the surrounding microenvironment [2]. Upon detection of any insult to brain tissue, microglial cells undergo a process of activation that entails changes in their shape and function. Cytoplasmic processes shorten and thicken until cells appear to be indistinguishable from blood-borne macrophages, begin producing a myriad of cell-signalling molecules and receptors, and acquire the capacity of antigen presentation, phagocytosis, migration and proliferation [3, 4]. Activation can be triggered by a broad variety of stimuli including hypoxia, accumulation of insoluble molecules, infective agents or the contact with neoplastic cells [4]. In anaplastic astrocytomas and glioblastomas, microglia contribute significantly to the total tumour mass but the fact that neoplastic cells manage to survive and grow in their presence indicate the failure of normal defence mechanisms [5, 6]. The causes of poor microglial response to tumour cells are still unclear although recent studies have demonstrated glioma-infiltrating microglial cells show an impairment of antigen presenting functions [6–10].

The peripheral benzodiazepine receptor (PBR) is one of the earliest and most commonly expressed molecules during microglial activation in inflammatory, degenerative, vascular and infective CNS diseases [3, 5, 11]. For this reason, high levels of PBR are generally considered a marker of microglial activation [5], and the PBR-specific ligand [^{11}C](R)-PK11195 is widely used in positron emission tomography (PET) studies to trace microglial infiltrate as an in vivo indicator of tissue damage [11]. Also known as PK-11195 binding protein or translocator protein, the PBR is an 18 kDa molecule consisting of a five helices spanning the membrane lipid bilayer of the outer mitochondrial membrane and forming a heterotrimer together with a voltage dependent anion channel and an adenine nucleotide transporter [12, 13]. The PBR is expressed in several normal tissues with the highest levels in gonads and cortical cells of adrenal gland [14, 15] and its major function is to actively transport cholesterol and proteins through the mitochondrial membrane [13]. The actual role of PBR in microglial cells is still to be elucidated although recent studies in vitro [16] and animal model [17] suggested that it may exert a pro-inflammatory function. Interestingly, several studies have found high-PBR levels in tumour cells of glioblastomas and to a lesser extent of anaplastic astrocytomas [18] but none of them have mentioned glioma-infiltrating microglial cells as possible source of PBR.

Here, we present the results obtained during a feasibility study designed to explore the expression of PBR in human astrocytic tumours and the diagnostic use of [^{11}C](R)-PK11195 PET-scan in neuro-oncology. We investigated PBR in vivo using [^{11}C](R)-PK11195 PET imaging and with immunohistochemistry in tumour tissue. Tumour-infiltrating microglial cells were also characterised for the expression of molecules involved in antigen presentation and cytotoxic activity and results obtained in astrocytomas were compared with cases of multiple sclerosis (MS) and Parkinson's disease (PD), which are known to contain a substantial amount of activated microglia.

Clinical findings

Case 1

This 27-year-old male presented with a 2-month history of seizures. MR-scan (1.5 Tesla Sonata scanner, Siemens, Erlangen, Germany) demonstrated a lesion of the right temporal lobe, which appeared inhomogeneously hypointense on T1-weighted sequences and hyperintense in the T2-weighted sequences. Only minimal enhancement was observed after administration of gadolinium (Fig. 1a). No therapy has been given prior to surgery but 800 mg/day of valproate.

Case 2

This 53-year-old female presented with a 4-year history of progressive dysesthesia in right upper and lower extremities. MRI-scan revealed a right fronto-insular intra-axial lesion that was inhomogeneously hypointense in T1-weighted images and hyperintense in the T2-weighted sequences (Fig. 1c). Only mild diffuse enhancement was seen. No radiotherapy, chemotherapy or corticosteroid therapy were administered prior to the PET scanning and surgical resection.

Both patients underwent surgical debulking and samples were submitted for pathological examination. This study was approved by the Ethics Committee of the Kyoto University Graduate School of Medicine (No. 420) and by the Central Ethics Committee, London UK (No 05/Q0401/3), and informed consent was obtained from both patients.

Materials and methods

PET imaging acquisition and analysis

Both patients underwent [^{11}C](R)-PK11195 PET scan (Advance, General Electric, Milwaukee, WI, USA) and a

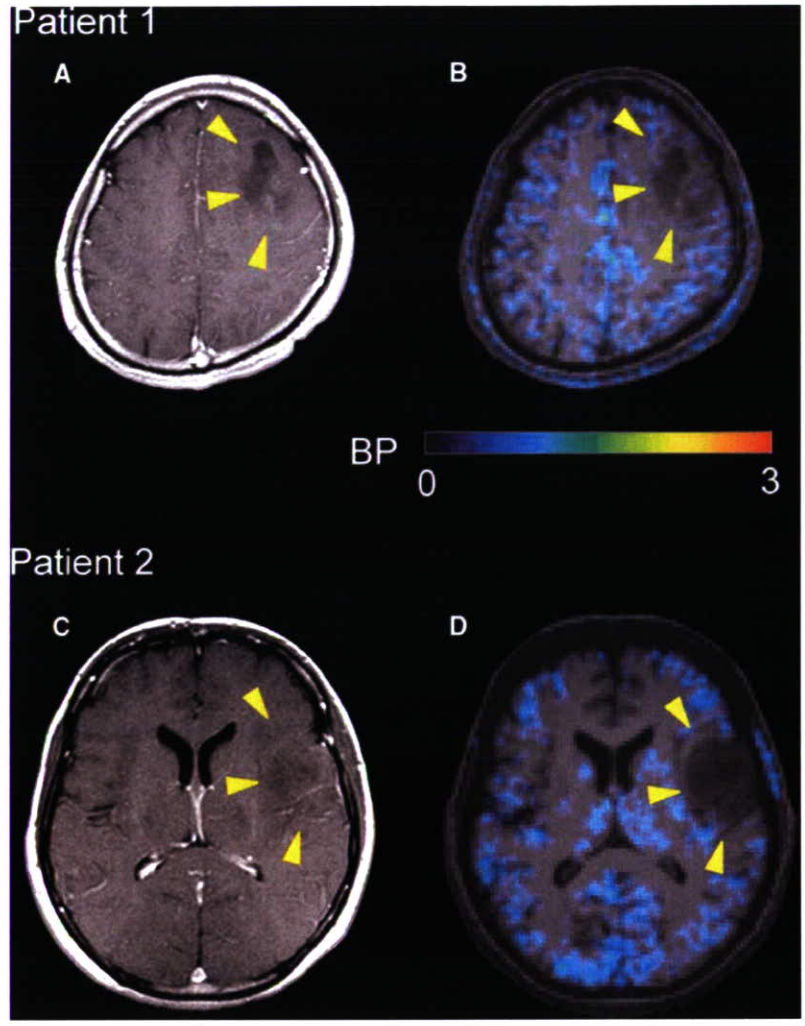

Fig. 1 Gadolinium-enhanced MRI (**a, c**) and [^{11}C](R)-PK11195 PET superimposed on 3D MRI (**b, d**). The intensity of the lesions is low in the T1-weighted images with minimal contrast enhancement (**a**, patient 1, left frontal region; **c**, patient 2, left frontotemporal region; *arrowheads*). Both lesions show decreased [^{11}C](R)-PK11195 binding than the normal grey matter (**b, d**; *BP* binding potential)

three-dimensional T1-weighted MRI (magnetisation prepared rapid acquisition gradient-echo sequence; TR/TE, 2000/4.38; 3 Tesla Trio scanner, Siemens) prior to surgery. PET study was performed in three-dimensional acquisition mode as previously reported [19]. A 6 mCi bolus of [^{11}C](R)-PK11195 was injected intravenously into the patients 30 sec after the acquisition scan started. Dynamic PET data were acquired over 60 min as 18 temporal frames. Attenuation correction factors were determined using a 15-min eight-emission scan. Data were reconstructed with a ramp filter. Kinetic modelling was performed by Logan graphical analysis without blood sampling [20]. We used the time-activity course of the radioactivity in a reference tissue (normal grey matter contralateral to the tumour) of each patient as the input function. The binding potential (BP) was calculated as BP = DVR - 1, where DVR is the ratio of the volume of distribution (DV) in the region of interest to that in the reference region. The DVR was calculated as the slope of the Logan plot that was obtained by linear regression analysis. Finally, PET images were coregistered onto 3D MRI images by using the mutual information algorithm implemented in SPM2 (Wellcome Department of Imaging Neuroscience, UCL, London, UK).

Pathological investigation

Surgical samples were fixed in 10% buffered formalin and paraffin embedded. Five-micron sections were cut and stained with haematoxylin-eosin (HE). Immunohistochemistry was performed using the avidin–biotin complex/peroxidase (ABC) method with antibodies directed against PBR (monoclonal clone 8D7; dilution 1:200; kindly supplied by Dr. Pierre Casellas, Department of Immunology-Oncology, Sanofi Synthelabo, Montpellier, France), MHC class II antigen (HLA-DR) (MHCII) (Dako Cytomaton, Glostrup, Denmark; clone CR3/43; dilution 1:200), CD80 (B7.1) (Abcam, Cambridge, UK, clone MAB104 dilution

1:100), CD86 (B7.2) (Sigma, Deisenhofen, Germany, clone B72-H2, dilution 1:100), Tumour Necrosis Factor alpha (TNF-alpha) (Chemicon, Termecula, CA, USA, clone 195, dilution 1:200), inducible nitric oxide synthase (iNOS) (R&D, Wiesbaden, Germany, clone 2B2-D2, dilution 1:50) and cyclooxigenase 2 (COX-2) (BD Transduction Lab, Palo Alto, CA, USA, clone 33, dilution 1:250). For all antibodies, the sections were pretreated in 1 mM EDTA (pH 8) for 20 min in microwave oven at 500 W.

The epitope recognised by the anti-PBR antibody corresponding to the cholesterol binding domain (amino acids 158–169) [12, 21] was compared with all the known human proteins (Blast/Fasta; www.pir.georgetown.edu) and no match was found other than with the three PBR isoforms. The protocol for PBR was assessed using normal adrenal gland that constitutively contains high level of the protein [15]. We also tested the anti-PBR antibody with Western-blot analysis with extracts from adrenal gland and normal frontal cortex. A standard protocol was followed [22].

The extent of expression of microglial PBR in non-neoplastic CNS diseases was examined in active demyelination from three post-mortem brains with MS, and in the substantia nigra of three brains with PD. Brains with MS were donated to the UK MS Tissue Bank and PD cases were donated to the UK PD Society Tissue Bank, both at Imperial College, London. These samples were previously immunostained for MHCII antigen and they were known to contain activated microglial cells. Lymphocytes, neutrophils, endothelial cells and smooth muscle cells present within tumour tissues were considered internal positive controls, as they are known to constitutively express PBR [13, 23]

Evaluation of microarray datasets

The differences between microglial in astrocytomas and non-neoplastic CNS diseases were also explored by examining the expression profile of four anaplastic astrocytomas, which are part of a group of gliomas we have studied with expression microarrays (Affymetrix, Santa Clara, CA, USA, U-133 Plus 2; available online GEO database, GEO submission GSE2817) [for details see reference 24]. Tumours were compared with eleven normal temporal lobes removed in course of surgery for intractable epilepsy. Anaplastic astrocytomas and normal temporal lobes were characterised for the extent of microglial infiltrate using MHCII antigen and for the expression of PBR and COX-2 (immunohistochemical stains are described above). As example of a non-neoplastic CNS condition, we explored a dataset obtained from the substantia nigra of nine PD cases (Affymetrix, U-133 A) [25]. Cases of PD were compared with the expression profile of the substantia nigra of seven age-matched normal brains. The three PD cases used for immunohistochemistry were part of the group used for expression microarrays. We investigated the expression of molecules involved in microglial response including MHC class II antigen (HLA-DR), CD40, CD80 (B7.1), CD86 (B7.2), CD40, Toll-like receptors (TLR) 1–8 and 10, and TNF-alpha receptors 1. Astrocytomas and PD cases were compared to the respective control tissue. Details on microarray data processing and normalisation are reported in the respective references [24, 25]. Statistical analysis was performed using a Mann–Whitney test. Analysis of expression profiles did not include other molecules contributing to microglial immune response such as TNF-alpha, iNOS and COX-2 because probes for these molecules are not contained in the Affymetrix arrays.

Results

PET findings

[^{11}C](R)-PK11195 PET studies revealed that the binding of the ligand was markedly lower in both tumours than in the contralateral grey matter [Figs. 1b, 1d] [Fig. 2]. The tumour/normal grey matter ratios of the integrated radioactivity and BP in each patient were 0.67 (patient 1) and 0.51 (patient 2), and 0.68 (patient 1) and 0.51 (patient 2), respectively.

Validation of the anti-PBR monoclonal antibody

Normal adrenal gland demonstrated expression of PBR in the cells of the *zona glomerulosa*, *reticularis* and *fasiculata*

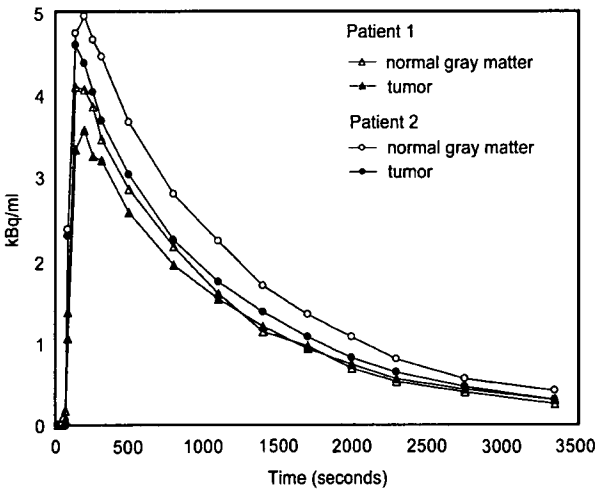

Fig. 2 Regional time activity curves (*TAC*) extracted from the dynamic [^{11}C](R)-PK11195 PET data of both patients (no decay correction). In both cases, the TAC is lower in astrocytomas than that in the reference cortical region

and the sections of normal brain showed expression in a few perivascular macrophages. Western-blot analysis revealed a band of 18 kDa in both extracts corresponding to the known molecular weight of the PBR. Signal seen in brain tissue was much weaker than signal in adrenal gland.

Pathological findings

Both tumours were diagnosed as anaplastic astrocytoma (grade III, WHO classification) [26] by two independent neuropathologists. They were composed of astrocytic cells with fibrillary cytoplasm and moderate to severe nuclear pleomorphism. Mitotic activity was brisk in both cases. No necrosis and, vascular and endothelial proliferation was seen (Fig. 3a). As seen with the immunoreaction for MHCII, both tumours contained a substantial number of activated microglial cells and macrophages that accounted for ~40% of the total number of cells (Fig. 3b). The anti-PBR antibody demonstrated expression in a few tumour cells and no expression in microglia (Fig. 3c) PBR-positive lymphocytes were observed within the vessels and leptomeninges (Fig. 3d). Leptomeningeal arteries showed PBR expression in endothelium and smooth muscle cells of the tunica media whereas normal vessels entrapped with tumours vessels showed weak expression. In both cases, some microglial cells expressed CD80 and CD86. TNF-alpha was present in a few microglial cells mainly located in the subpial tissue whereas iNOS and COX-2 were only observed in a few neoplastic cells.

The three cases of MS showed intense PBR expression in activated microglial cells surrounding active plaques as well as in microglia and macrophages within areas of demyelination (Fig. 4a). Strong expression of PBR was also seen in activated microglia in the substantia nigra of the three PD cases (Fig. 4b). In all the samples examined we observed PBR expression in the wall of several medium

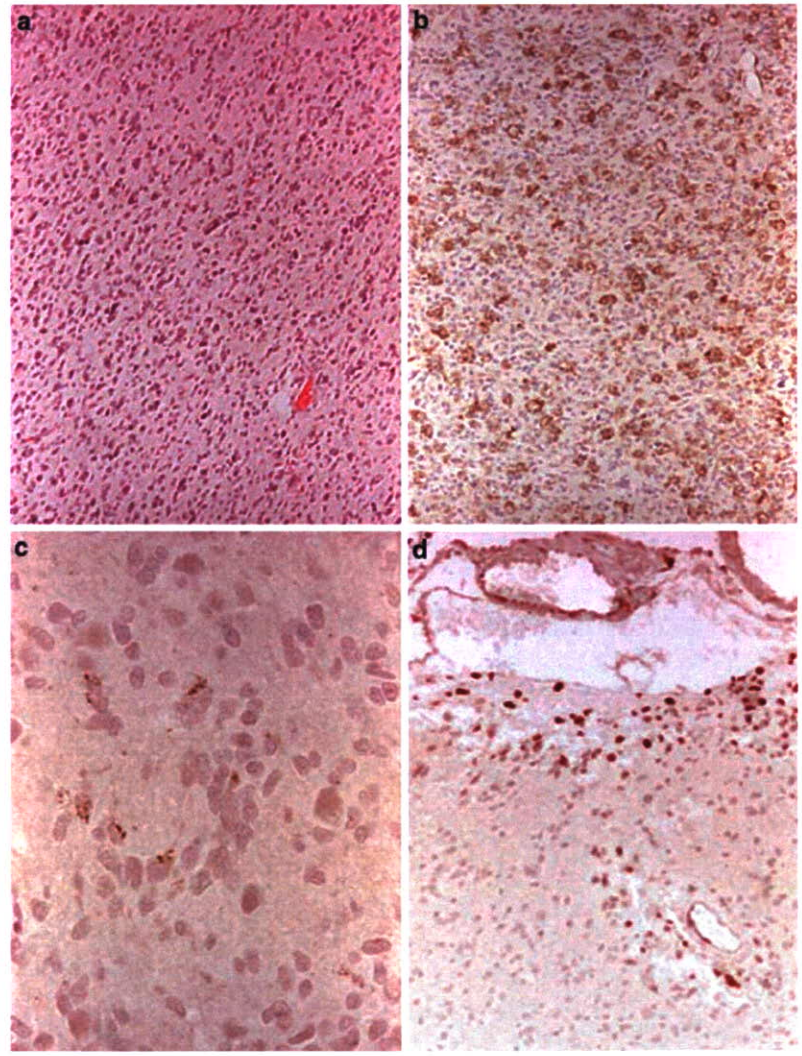

Fig. 3 The tumour in patient 1 shows the features of an anaplastic fibrillary astrocytoma (**a**; HE staining; × 10). The immunoreaction for the MHC class II antigen demonstrates a considerable number of activated microglia (**b**, × 10). PBR is expressed in a few tumour cells but it is undetectable in microglia (**c**; patient 1 × 25). PBR expression is observed in the leptomeningeal lymphocytes and leptomeningeal vessels (**d**, patient 1, × 4)

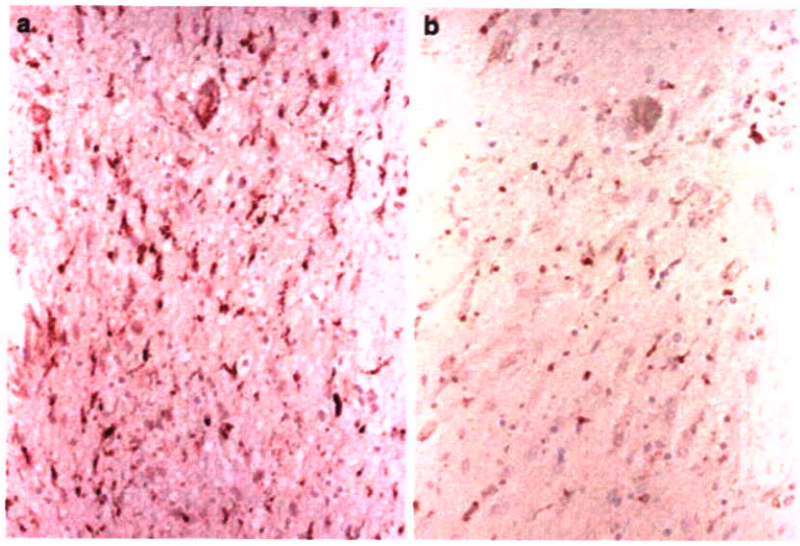

Fig. 4 Intense expression of PBR is seen in activated microglia in an active MS plaque (**a**) and Parkinson's disease (**b**, nigra) (ABC/peroxidase)

sized and small arteries. Both MS and PD cases featured expression of CD86, TNF-alpha, iNOS and COX-2 in microglial cells.

Evaluation of microarray datasets

Immunohistochemical stains for MHCII revealed a diffuse microglial infiltrate in the four anaplastic astrocytomas used for microarrays analysis compared to normal control tissue. The PBR was expressed in tumour cells and in a few microglial cells. Notably, all the tumours showed a considerably high number of MHCII-positive microglial cells than PBR-positive and COX-2 positive microglia. Expression analysis of anaplastic astrocytomas showed levels of PBR as low as control brains. Expression of MHCII, CD86 and TLRs 4 and 5 in anaplastic astroctyomas were significantly higher than normal brains ($P < 0.1$) whereas CD80 and CD40 were high but expression values did not reach significance. TNF-alpha receptor 1 was only mildly elevated and TLRs 1–3, 6–8 and 10 were as low as normal brain. In the substantia nigra of PD cases, the expression of PBR, TLRs 4 and 5 and TNF-alpha 1 receptor were increased compared to normal nigra ($P < 0.1$); MHCII, CD40, CD80 and CD86 showed borderline levels compared to controls. All values of expressions were normalised to the respective control tissue (Fig. 5).

Discussion

We observed that activated microglial cells infiltrating two cases of anaplastic astrocytoma do not express PBR. This finding is interesting because it differs from all imaging studies with [^{11}C](R)-PK11195 [11], microarray studies [5], studies in vitro [27, 28], animal model [3, 29, 30] and post-mortem brains [22] that showed high expression of PBR in activated microglia in a variety of inflammatory, degenerative, infective and vascular CNS disorders. Our approach of combining the evaluation of PBR using [^{11}C](R)-PK11195 PET-scan and immunohistochemistry offered the advantage of studying the binding capacity of this molecule *in vivo* and, on tissues its distribution in the cell types constituting the two astrocytomas without the

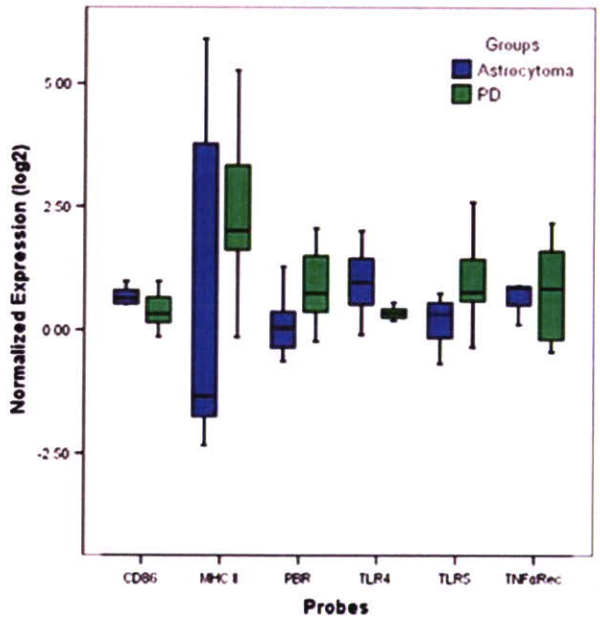

Fig. 5 This diagram demonstrates the expression of mRNA of PBR, MHCII, CD86, TLR4 and 5 and TNF alpha receptor 1 in anaplastic astrocytomas (*blue*) and PD (*green*). Expression is normalised to the control tissue